

Contents

1	Introduction	1
2	Background theory & literature review	3
2.1	Deep Learning	3
2.1.1	Convolutional Neural Networks	4
2.1.2	Drawbacks of deep-learning	5
2.2	Interpretability techniques	5
2.2.1	Feature visualization	6
2.2.2	Saliency maps (or how to assign importance scores)	8
2.3	Deep Learning in biology	9
2.3.1	CNNs on biological sequence data	10
2.3.2	Interpretability techniques on biological sequence problems	11
2.4	Protein Secondary Structure Prediction	13
2.4.1	Input features	14
2.4.2	Targets	15
2.4.3	State of the art	16
3	Methods	19
3.1	Dataset	19
3.2	Network of study	20
3.3	Feature visualization	21
3.4	Saliency maps	22
3.4.1	Extracting information from saliency maps	22
3.5	Open-source	22
4	Results & Discussion	23
4.1	Outlier analysis	23
4.2	Feature visualization: first-layer filters	24
4.3	Saliency maps on inputs	25
4.3.1	Analysis of amino-acids and <i>pssm</i>	25
4.3.2	Sequence-specific saliency maps	26
4.3.3	Class-specific and <i>pssm</i> -specific saliency maps	27
4.4	Final discussion	30
5	Conclusions	33
A	First-layer filters	35

B Saliency map aggregations	37
C Project planning	39
Bibliography	41

Chapter 1

Introduction

Although the recent arrival of deep learning has introduced unprecedented improvements in many fields, it also brings techniques that are remarkably difficult to understand. Many layers of neurons stack on each other and build complex networks of interactions; the information is distributed, and units are meaningless when we look at them isolated. The outcome emerges from the interaction of them all, and this indivisibility is what makes them so hard to grasp. Without being able to look inside, debugging efforts are futile, and we lose the benefits of learning from the acquired representations.

Biomedical research is one of the fields in which deep learning has overcome previous techniques. This is partly due to the complex interactions that occur in the networks been studied there, from gene regulatory networks in the molecular level to macro-ecosystems. One of the sub-domains where deep learning excels is sequential data at the cellular level, i.e. DNA, RNA and protein chains. Despite its good performance results, the lack of interpretability is again a significant issue since we do not fully understand the underlying processes being modelled and uncritically accepting the outcome is not the best option. If experts in the field can somehow verify what the system is doing, they will be able to contrast it with their knowledge to both spot spurious rules being learned and update their knowledge with new valuable pieces.

The field of image processing, which is one of the earliest to embrace deep learning, has already started to work on the development of interpretability techniques. They focus on capturing the representations that are formed in the intermediate layers to understand what kind of features are learned at different stages (*feature visualization*), as well as exploring which sections of the inputs contain the most crucial information for the system to make a decision (*saliency maps*). Although there have been a few attempts to bring them to biological sequence problems, there is still much room for improvement. This project aims to explore ways to implement saliency map techniques into biological sequence problems; more specifically, into protein secondary structure prediction, one of the canonical sequence-to-sequence prediction problems in cellular biology.

Chapter 2

Background theory & literature review

2.1 Deep Learning

The Deep Learning term was created in contrast to “shallow” Machine Learning. Typical machine learning algorithms involve processing the information from the input into a different *feature space* in which the data is represented in a more structured way. With deep learning, this process is repeated several times allowing for feature spaces with higher-level abstractions that have more power to learn complex relations in the input (Goodfellow et al. (2016)). In the beginning, neural networks would only have a single hidden layer of neurons. Theoretically, one layer should suffice for learning any continuous function —according to the *universal approximation theorem* (Cybenko (1989))— provided that the network has enough hidden units. However, the number of necessary units for reaching a certain accuracy can grow exponentially with the input space (Barron (1993)), which can only be alleviated by increasing the depth of the system. Bigger networks were hard to train at the beginning because of an increased number of parameters that significantly extend the computation training time, a higher risk to over-fit due to their increased power, *vanishing gradients* —lower-layer parameters receive weak signals from the error and could barely learn— and their need for vast amounts of data, not readily available at the time. Such problems have been recently overcome thanks to the use of Graphical Processing Units (GPUs) that boost computing speed, techniques such as *dropout* (Srivastava et al. (2014)) and *batch normalization* (Sergey Ioffe and Christian Szegedy (2015)) that add extra regularization, the inclusion of Rectifying Linear Units (ReLUs) as non-linear functions, and the profuse amount of data available thanks to the Big Data broader movement. Since then, its use has been growing, and it has spread to many research fields, with high performance in image classification —improvement of 10% from previous methods (Krizhevsky et al.

(2012))—, speech recognition —more than 5% improvement (Veselý et al. (2013))— and language translation —more than 1 point BLEU score increase (Cho et al. (2014))—.

Multi-Layer Perceptrons (MLPs), Recurrent Neural Networks (RNNs) and Convolutional Neural Networks (CNNs) can be found among the most widespread deep networks. MLPs are composed of consecutive layers of fully-connected units that pass the information in one direction and are hence called *feedforward*. RNNs differ from MLPs in that units are also allowed to have connections to themselves. Instead of having an input vector that produces an output in a *one-go* fashion, RNNs store information from previous inputs and are particularly well-suited for inputs that are sequentially correlated. CNNs slide a local filter throughout the input, obtaining location-invariant information. A more in-depth look into this kind of network is shown in the following sub-section.

2.1.1 Convolutional Neural Networks

As mentioned above, CNNs (LeCun et al. (1998)) work by having filters that operate along some spatially correlated input. Filters are small patches that hold one weight per position. They perform element-wise multiplication with a patch from the input of the same size and add them up into a single output that is located at its centre. A non-linear function is then applied to the output space in order to obtain more expressive models. By performing this operation at all possible overlapping input patches, they produce a feature map that is somehow linked to the underlying input space. Since the same small filter is applied to the whole input space, they capture features or motifs that are location-independent. Moreover, just a small set of weights is used for an arbitrarily large input space, making them much more efficient and able to build deeper networks.

When defining a convolution operation, two extra parameters need to be taken into account: *padding* and *strides*. Padding consists of augmenting the input space by adding margins with zero value. It is especially useful for preserving the size of the input into the feature space, which is done by adding a margin of half the filter size. The strides define the size of the steps taken every time the filter is slid, determining the amount of overlapping in the produced feature map. Figure 2.1 shows a simple schematic of how a filter with padding and strides works.

A convolutional layer typically includes a few sets of filters with varying size, producing a set of feature maps. Convolutional layers stack onto each other, building more and more abstract concepts. They can also be interleaved by pooling layers that shrink the space by applying operations to their inputs in a similar fashion as the filters. Typical pooling operations are *max-pool*, which takes the maximum value in a patch, or *average pooling*, which averages over all units in the patch. The whole structure can be capped

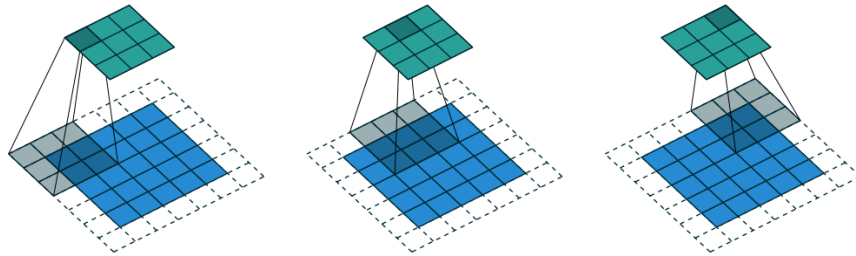


FIGURE 2.1: *Convolution operation with a 3×3 filter, padding of 1×1 and strides of 2×2 .* The blue cells represent the input space, the white ones are the result of padding, and the green cells form the output feature space. The filter operation is performed on the shaded input cells and produces the shaded output cells. Due to the strides, the filter jumps two positions while sliding. Figure reproduced from [Dumoulin and Visin \(2016\)](#).

by a fully-connected MLP that performs a classification task, and all the weights trained by *backpropagation*.

The use and performance of CNNs have grown in the last few years, thanks to more sophisticated network structures ([Szegedy et al. \(2016\)](#); [Huang et al. \(2017\)](#)). They have had particular success for the tasks of image classification, object detection, text recognition, speech recognition, natural language processing, among others ([Gu et al. \(2017\)](#)).

2.1.2 Drawbacks of deep-learning

Despite the benefits of improved performance, deep learning still finds some resistance in the broader public due to varied reasons. First, its higher complexity imposes a steeper learning curve. Second, the lack of a mature set of tools and samples due to its novelty makes its access difficult —although there has been an increasing, active community that is swiftly covering these needs—. Third, the high computational times are only partially relieved by GPUs. Last, deep networks are hard to interpret and obtaining information from the middle layers is not straightforward. Their *black box* behaviour hinders developers from understanding both where networks fail and why specific outputs are produced. This drawback has been of big concern lately, and the research community has switched the focus to developing *interpretability techniques* to overcome it.

2.2 Interpretability techniques

Due to the *black box* nature of deep non-linear networks, they cannot be easily interpreted by humans. It is different from previous shallow, linear models, where a look at the weights can already give an idea of what the network is doing and which inputs

are more important. Unfortunately, linear models are limited in their power and cannot tackle complex problems, so we are often forced to employ deep alternatives and sacrifice the interpretability benefits. For this reason, in recent years researchers have been developing interpretability techniques that can increase our understanding of deep networks. Although still not as clear as with linear models, we can get some insights of what deep networks are learning and why they take their decisions. Two main groups of techniques have emerged in the literature: *feature visualisation* and *saliency maps* ([Olah et al. \(2017\)](#)). While the first group focuses on the latent spaces that are formed in the hidden feature layers, the second group aims to detect which parts of the input had more relevance when performing a classification.

2.2.1 Feature visualization

Feature visualisation techniques try to understand what is learned at each layer. A typical example happens with CNNs for image recognition. There was some intuition that the base layers would look for simple patterns, like edges or dots, and successive layers would build more complex patterns (eyes, leaves) and end up with full objects at upper neurons ([Mordvintsev et al. \(2015\)](#)). Visualizing first layers was a common practice by then, but it could only reach the basic edge detection level. This is not as useful since it is a feature shared by most image recognition networks, so other methods of visualisation arose.

Linear combination of filters

The most naive approach to represent higher-level filters is to stack them onto lower-level ones and get visualisations similar to the low-level filters, as performed by [Lee et al. \(2009\)](#), who built each higher filter with the lower-level ones that held the highest weights. Despite its simplicity and unprecedented results for the time, this technique presents some problems. [Erhan et al. \(2009\)](#) point out that the method ignores non-linearities and that “it is not clear how to automatically choose the appropriate number of filters to keep at each layer.”

Activation maximization

Activation maximisation techniques were first coined by [Erhan et al. \(2009\)](#) and hold a different approach than previous methods: instead of looking at filters they take the visualisations to the input space. The goal is to find inputs that maximise the activation of the specific neuron (or set of neurons) that is inspected. The simplest way of doing so would be finding which samples from the training or test set achieve this and try to figure out what they have in common. This simple idea may provide some intuition about the

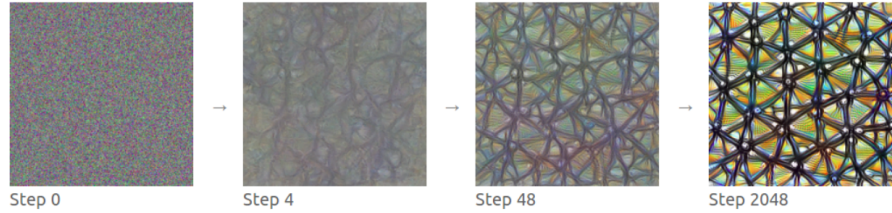


FIGURE 2.2: *Activation maximization method*. The process starts with random noise and performs gradient ascent to find the input sample that maximizes the activation of a unit (or a channel, in this case). Figure reproduced from [Olah et al. \(2017\)](#).

neuron, but it is barely as good with networks that are trained in tasks other than image recognition since it may be much harder to spot the similarities between samples that are not as intuitive as images. Besides, it is not straightforward how to obtain the key common features from the images, and we cannot know how many samples per unit should be gathered and inspected.

[Erhan et al. \(2009\)](#) came out with a more principled way of finding maximally activating samples outside of the dataset. They proposed to artificially produce them by starting with random noise and tweaking the input space in the direction that increases the activation via *gradient ascent* while keeping the norm constant. Since most neural networks learn by backpropagation, they are already differentiable, and the calculation of the gradients can be recycled for this technique. Formally, we can define the optimisation problem as

$$x^* = \arg \max_{x \text{ s.t. } \|x\|=\rho} h_{ij}(\theta, x), \quad (2.1)$$

where x is an input vector, h_{ij} the activation unit we want to visualise, and x^* the maximally activating sample. A visual instance of this process can be seen in Figure 2.2.

This technique brings the benefit of keeping the most relevant parts that are captured by the unit and discard all the non-relevant information. It can also be easily applied to groups of neurons, such as channels, layers or other arbitrary collections, and it can be applied at different stages of the training process in order to visualise how the learning evolves. However, it also has some drawbacks: the optimization function is non-convex, and the algorithm can arrive at different local minima, so special techniques need to be added to find all the relevant ones ([Nguyen et al. \(2016\)](#); [Olah et al. \(2017\)](#)), the gradient ascent requires setting a stopping criterion and a learning rate, and the process can produce highly unrealistic samples. This last issue could be potentially mitigated by the introduction of duly prior constraints, such as “neighboring pixels needing to be correlated” in natural images ([Mordvintsev et al. \(2015\)](#)). [Montavon et al. \(2018\)](#) materialise the inclusion of this prior knowledge with an *expert term* in Equation 2.1. He argues that its determination is crucial in the quality of the resulting sample, and suggest seeking slightly under-fitting expert terms.

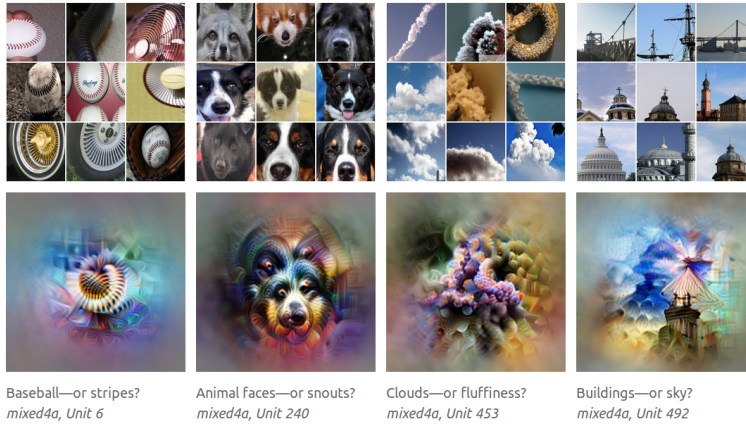


FIGURE 2.3: *Maximally activating samples from training/test set (above) and activation maximization outcome (below) for four different units.* A single activation maximization local minimum does not capture all the variety of the neuron, so a multi-faceted set of them should be sought. Figure reproduced from [Olah et al. \(2017\)](#).

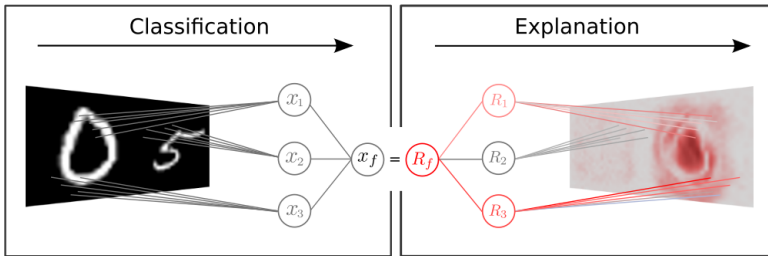


FIGURE 2.4: *Basic sample of a saliency map.* Here, the network is detecting the digit zero on the left and the pixels that contributed to the classification are highlighted on the right. Image reproduced from [Montavon et al. \(2017\)](#).

2.2.2 Saliency maps (or how to assign importance scores)

Saliency maps are a series of techniques that are developed in order to reveal which parts of an input sample are mainly responsible for the output decision that the network makes. They can be a powerful tool both for spotting spurious rules learned by the system (in cases where we can easily judge whether a result is wrong) and learning more about the underlying processes (when we cannot explain the reason of a result). An example of a saliency map visualisation can be seen in Figure 2.4.

The most straightforward approach to achieve this goal is performing a sensitivity analysis, i.e. making modifications of the input sample and register how variations in each input unit (or combinations of them) affect the output of the system. These techniques can be applied to other different outputs from the post-softmax to give ideas of intermediate layers as well. They can be grouped by the name *perturbation-based approaches*, and they all face the same problem: when the input space is moderately big, exploring a decent amount of variations and combinations of input units is intractable, or quite computationally expensive at the least. A second concern relates to its inability to capture the importance of neurons that are already saturated. One example of such methods

specifically applied to CNNs is DeConvNets (Zeiler and Fergus (2014)), a machine that assigns scores to specific patches of the input image based on their contribution.

The second series of approaches—which mostly overcome the computational problems—are based in back-propagation. The most intuitive idea behind them is that the gradient of an input already tells you its sensitivity (how much the output will change from a small change in the input), and it can be calculated on a single back-prop operation instead of performing a profligate number of feed-forward passings with small variations in the inputs (Shrikumar et al. (2017)). It can be thought as a linear approximation of the function around the sample point x_0 by applying first-order Taylor expansion, as introduced by Simonyan et al. (2014):

$$f(x) \approx wx + b, \\ w = \left. \frac{\partial f}{\partial x} \right|_{x_0}. \quad (2.2)$$

Some other similar methods were developed, with their main differences residing in the treatment of ReLUs in the back-propagation process, such as *guided backpropagation* (Springenberg et al. (2014)). However, they do not give solid explanations for assigning importance since they do not hold basic principles such as conservation (all the importance scores at any layer should sum up to the output score). This principle was later introduced by Bach et al. (2015) with the *Layer-wise Relevance Propagation* (LRP) method, although it has been later discussed that the rules it follows are mainly heuristic and more principled ways of choosing the rules have also been suggested (Montavon et al. (2017)). It was later proven that these rules were equivalent to having the element-wise multiplication of the original saliency maps by the input itself (Shrikumar et al. (2016)).

Finally, a last wave of methods proposes including a reference point and hence properly accomplishing the Taylor approximation. Main examples are *integrated gradients* (Sundararajan et al. (2017)), Deep Taylor Decomposition (Montavon et al. (2017)), and DeepLIFT (Shrikumar et al. (2017)). They overcome problems of previous methods such as saturation or discontinuities in the gradients, although they bring the extra difficulty of choosing an appropriate reference point.

2.3 Deep Learning in biology

Recent advances in measuring techniques have produced vast amounts of biological data, which usually is highly dimensional and reflects incredibly complex underlying processes. Such settings demand more powerful models than before, and deep learning has found there a natural field in which to thrive. Among the most prominent application domains in which it has been successfully implemented, we can find images (bioimaging, medical

imaging), brain/body-machine interfaces (*BMIs*) and *omics* (Mahmud et al. (2018)). The *omics* term refers to research on sequence data at the cellular level, namely DNA (*genomics*), RNA (*transcriptomics*) and proteins (*proteomics*), and their interaction (*multiomics*). Sequential data is particularly interesting for deep learning since it is among the kinds of problems where it excels, particularly with the application of RNNs and CNNs. They have been widely employed for structural annotation of the DNA chain (Jones et al. (2017)), protein classification (Min et al. (2017)), splicing code (Mamoshina et al. (2016)) and transcription factors (Ching et al. (2017)), among others.

2.3.1 CNNs on biological sequence data

As it has been mentioned in Section 2.1.1, CNNs are mostly useful for data that is spatially correlated, which is the case of sequential data. This is because that they can accept input sequences of arbitrary size and they can capture motifs in them irrespectively of where they are located (Jurtz et al. (2017)). While applying convolutions to 2D input images is a well-known task, it is not as common to apply them to one-dimensional data. It is nevertheless fairly intuitive. Filters cover the whole depth (channels) of the data and have variable width depending on the number of adjacent positions to be captured. Filters slide only in the direction of the sequence, with possibilities of different strides and padding, as in normal 2D convolution. A 1D convolution operation transforms the 2D input sequence x , with length L and depth D , into the 1D feature sequence z . Each element of z is computed as

$$z_i = f \left(\sum_{k=0}^D \sum_{j=-h}^h w_{jk} \cdot x_{i+j,k} + b \right), \quad (2.3)$$

with h being the half-width of the filter, w_{jk} and b the weights and bias variables of the filter and f the non-linear activation function. Many simultaneous convolution operations can be performed at any layer with varying parameters in order to obtain a 2D set of feature maps that will serve as input for the next layer.

While signal inputs contain real-value data, categorical sequences —such as DNA, amino-acid chains, or characters in a text classification task (Zhang et al. (2015))— are presented in their one-hot version, defining the depth of protein chains as 21 for proteins (the different possible amino-acids) and four for DNA and RNA (the four bases). Some extra depth can be added with additional known features of the elements, such as solvent accessibility or *pssm* values in the case of amino-acids.

There are two main ways in which to apply convolutions to sequence data depending on the problem: structural annotation or sequence classification. The first kind requires the network to assign a label or value to each of the positions in the input sequence, and therefore the network needs to maintain the input length throughout the convolution

layers. This can be done with half padding and strides of one. The second kind produces a single output (classification) for a whole sequence. Since it is usual to have sequences of different lengths (as proteins), doing so requires a flexible shrinking process that cannot be achieved by standard convolution and pooling operations with fixed reduction sizes. A length-invariant step reduction can be achieved by a global max-pooling that retrieves the highest value of a sequence feature map at a single channel, therefore producing a fixed-size vector that can be fed to a soft-max layer ([Jurtz et al. \(2017\)](#)).

2.3.2 Interpretability techniques on biological sequence problems

The biomedical field is one that particularly benefits from interpretable systems. On the one hand, the costs of false predictions is expensive when it comes to diagnosis, and finding spurious rule is of particular importance. On the other hand, inspecting what networks are learning can provide with valuable information about the underlying biological processes. Unlike image data, sequence properties rely sheerly on the arrangement of a limited number of possible elements, so finding which motifs lead to certain outputs is of particular relevance. Apart from this, having non-interpretable models can impinge the trust of experts in the biomedical field and deter them from using the deep learning versions if they are not able to understand them.

Feature visualisation methods

As discussed in Section [2.2.1](#), a first approximation to visualise hidden features is to inspect the filters of the first layer of a CNN. It gives a basic idea of which ground features the network is building, but it is unable to go further than that, so it only remains relevant for shallow structures. When it comes to sequential biological data, an efficient way to convey the information of the first-layer filters that is familiar to biology experts is utilising *Seq2Logo* charts ([Thomsen and Nielsen \(2012\)](#)). 1D convolutional filters can be represented in this way by pairing up their values with the amino-acid of the one-hot row they cover. Two samples of such representations can be seen in Figure [2.5](#).

Some authors have gone further by applying activation maximisation techniques as well. [Fontal \(2017\)](#) attempted to apply them for protein subcellular localisation prediction via gradient ascent on the pre-softmax units (s_i) with an L2 regularisation parameter, λ :

$$\arg \max s_i(x) + \lambda \|x\|_2^2 . \quad (2.4)$$

[Lanchantin et al. \(2016\)](#) applied them to TF binding-site classification of genetic sequences with the same method (with post-softmax) and found that 30% of the motifs thus found were matched in a public motif database. As a different means of visualising

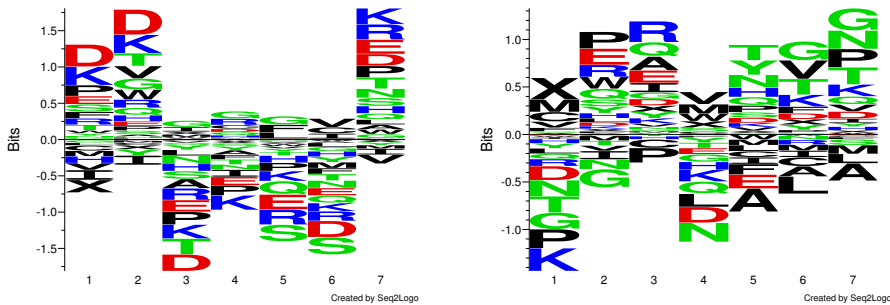


FIGURE 2.5: *Two first-layer filters for a protein sequence problem shown as Seq2Logo.* The x axis represents the span of the filters, which is seven in both filters presented here. While the left filter captures the appearance of specific amino-acids at the sides and not the centre, the right one resembles more an edge detector, with many of the amino-acids with different signs at each side.

hidden layer features, [Lanchantin et al. \(2016\)](#) also included temporal output scores for the RNNs models.

Saliency maps

As a simplified version of saliency maps, [Alipanahi et al. \(2015\)](#) and [Quang and Xie \(2016\)](#) spotted the segment in the input genetic sequence that had the highest activation of the first-layer filters and compared them to known motifs. This approach only makes sense as long as the network has a single layer, but cannot be applied to deeper networks.

[Alipanahi et al. \(2015\)](#) and [Zhou and Troyanskaya \(2015\)](#) showed how genetic mutations affected the output of their network, which is a natural way of performing perturbation-based approaches in the field. [Umarov and Solovyev \(2017\)](#) and [Fontal \(2017\)](#) substituted small windows of the sequence by random genetic code or the general amino-acid X, respectively, and assessed the differences in the output along the sequence by sliding such windows. [Kelley et al. \(2016\)](#) introduced known motifs at the centre of DNA sequences. All these can be categorised into the *perturbation-based approach* group and therefore need high computational times and cannot be exhaustive enough. For instance, how many window sizes and up to which range should be attempted to localise the influence accurately?.

Gradient-based approaches have barely been translated to the biological field yet. [Lanchantin et al. \(2016\)](#) include saliency maps with the form of gradient * input for TF binding site classification. They extracted the window with the highest score from each saliency map and compared them with a database of known motifs, matching almost half of the motifs thus produced. Figure 2.6 shows a sample of their saliency maps along with other interpretability methods implemented in their work.

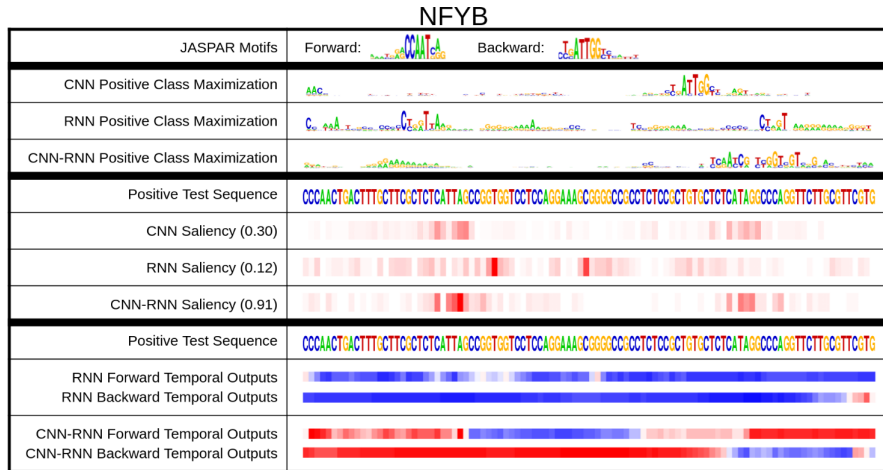


FIGURE 2.6: *Deep Motif dashboard including varied interpretability techniques for TF Binding Site classification.* This figure includes activation maximization methods (top), saliency maps (middle) and temporal outputs (bottom) for CNNs, RNNs, and a combination of both. Figure reproduced from [Lanchantin et al. \(2016\)](#).

Shrikumar et al. (2017) developed the new back-propagation based technique *DeepLIFT* and simulated a motif detection task within a genomic sequence to prove its effectiveness. Finnegan and Song (2017) utilised Markov chain Monte Carlo methods to withdraw samples from the maximum entropy distribution around a single sequence and assessed importance score by looking at the variance of the samples at each position. This technique was applied for previously trained DNA-protein binding CNN and proved to be better than DeepLIFT.

All these methods address classification problems where there is a single output (classification task) for the whole sequence, but, to the best of my knowledge, interpretability techniques have not been applied to structural tagging problems.

2.4 Protein Secondary Structure Prediction

Secondary structure prediction is a long-time studied problem that spans more than 50 years already (Pauling et al. (1951)). It has gone through many different stages as mathematical and computational methods evolved, being recently benefited from deep learning as well, to the point of approaching the theoretical accuracy limit (Heffernan et al. (2017))¹. Due to its long history, it has also been suggested that it effectively works as a problem benchmark for new techniques dealing with sequence data.

Predicting the secondary structure of a protein solely from its sequence can be seen as a middle step for tackling the much harder problem of predicting 3D structure. This last problem is of great importance in the biomedical field since protein structures are

¹Since there is 12% structure homology between proteins and transitions from coils to helices or strands are not clear-cut (Rost (2001)).

the principal indicator of their function, and obtaining this information can be of great use at drug design, disease treatment or early diagnosis, among others. However, due to the molecular scale, these structures cannot be easily measured, and any attempt to do so remains costly. A more feasible alternative is utilising computational tools to predict protein structures from amino-acid sequences alone having as reference the ones with known structure, as amino-acid sequences can be easily obtained from DNA sequencing data and they are widely available on heavily annotated public databases ([Dill and MacCallum \(2012\)](#)). From the nearly 85 million proteins whose sequences are known ([Hattori et al. \(2017\)](#)), we only know the structure of about 130 thousand ([Magnan and Baldi \(2014\)](#))).

2.4.1 Input features

The input to the system is an amino acid chain of length l . Since amino acids can be of any of 21 categories², the most natural way is to treat them as one-hot vectors, forming an input matrix of $21 \times l$. Other features of the amino-acids —such as solving accessibility or other physio-chemical properties ([Fauchère et al. \(1988\)](#))— can also be added to the end of the one-hot vector, adding thus extra-information that could potentially be important for making classifications. A typical approach to process the sequence involves inspecting it by *n-grams* (i.e. fragments of size n) and classify the middle amino-acid of each fragment with classical machine learning algorithms such as support vector machines (*SVMs*) or neural networks. With the arrival of CNNs and RNNs, the whole input matrix can be fed to the system, as they allow for inputs of varying lengths.

A key turning point in prediction performance appeared when Position Specific Substitution Matrices (*PSSM*) were added as extra features ([Yang et al. \(2018\)](#)). These values are originated from sequence alignment with *PSI-BLAST* ([Altschul et al. \(1997\)](#)) and express the probability of finding sequences that have a specific amino-acid substituted by another. Each amino-acid of the sequence has then 21 extra features that represent how likely each of the 21 types of amino acids is found at their place on similar sequences. This gives valuable information about mutations that do not change the structure of the protein (and hence its function) and are thus kept by evolution. In order to make the most use of this information with machine learning algorithms, it is usually filtered through a sigmoid function that maps the values between 0 and 1 ([Jones \(1999\)](#)), and it can be further normalised to zero mean and one standard deviation ([Busia and Jaitly \(2017\)](#)).

The combination of one-hot encoded (sparse) along with *pssm* (dense) features brings some problems for conventional machine learning algorithms: the dense part carries

²There are 20 standard types and the 21st amino-acid, X, is commonly used for representing all the unknown or non-standard ones ([Zhou et al. \(2018\)](#)). Other ways of handling non-standard amino-acids are also possible ([Fang et al. \(2017b\)](#)).

Q3 grouping		Q8 grouping		Explanation
α -helix	H	α -helix	H	Helix with 4 turns
		3_{10} -helix	G	Smaller helix with 3 turns
		π -helix	I	Bigger helix with 5 turns. Not as common.
β -sheet	B	β -bridge	B	Isolated β -bridge
		β -strand	E	Participates in β -ladders
		Turn	T	Turns that do not reach the minimum to be a helix
Coil	C	Bend	S	Curved piece
		Loop	L	Sometimes also categorized simply as coil (C)

TABLE 2.1: *Targets for the secondary structure prediction problem.* The simpler way of 3-class grouping was further expanded into eight classes by [Kabsch and Sander \(1983\)](#) in their Dictionary of Secondary Structure or Proteins (DSSP).

more information than the sparse one, so weights associated to this part of the input vector learn much faster. To deal with this, [Li and Yu \(2016\)](#) and [Zhou et al. \(2018\)](#) had the one-hot side of the input embedded into a denser representation through an MLP —as it is common in natural language processing ([Mesnil et al. \(2015\)](#))—, but reported only a small marginal performance improvement in doing that (0.5% and 0.4% Q8 accuracy, respectively). [Spencer et al. \(2015\)](#) reported an improvement of 2% Q3 accuracy by directly not including the one-hot amino-acids in their model, relying purely on the *pssm* scores.

2.4.2 Targets

Broadly, there are three kinds of local structures based on the hydrogen bonds formed between the amino-acids: *α -helix*, *β -sheet*, and *coil*. These were proposed by [Pauling et al. \(1951\)](#) when the protein secondary-structure problem was first defined. They have been the targets mostly used in the secondary structure prediction problem, and they are generally referred to as *Q3*.

A finer classification schema developed by [Kabsch and Sander \(1983\)](#), the *Dictionary of Secondary Structure of Proteins (DSSP)*, focuses in two smaller sub-units: *turns* and *bridges*. Repeating turns would form helices, and consecutive bridges create *ladders*, which in turn form sheets. Depending on how many of them are found together, different kinds of helices or strands could form, leading to a finer classification that comprehends eight classes in total: three kinds of helices, two sheets, and three coils. Having a more precise classification increases the complexity of the problem and has therefore been the focus of recent, more powerful deep learning approaches. This classification schema is commonly referred to as *Q8*, and an algorithm for its classification was also developed by [Kabsch and Sander \(1983\)](#). A detailed list of the classes can be seen in Table 2.1.

The natural way to format them for prediction is as one-hot vectors, allowing a softmax function to provide posterior probabilities, $p(Q|x)$. Networks are typically trained

using cross-entropy between targets and predictions, and the most commonly used performance score is accuracy, as the percentage of residues correctly classified. Some other performance measures include per-class precision and recall ([Wang et al. \(2016\)](#)), ROC Area Under the Curve ([Hattori et al. \(2017\)](#)), Matthews correlation coefficient ([Fang et al. \(2017b\)](#)), Person's Correlation Coefficient ([Jurtz et al. \(2017\)](#)), or Segment of Overlap ([Wang et al. \(2016\)](#)).

2.4.3 State of the art

Secondary structure prediction problem has a long history, with first approaches mainly rooted in statistics ([Chou and Fasman \(1974\)](#)). Breakthroughs can be found with the first implementations of neural networks ([Qian and Sejnowski \(1988\)](#)) and the inclusion of *pssm* values as inputs ([Rost and Sander \(1993\)](#)). Early neural network approaches included mainly shallow networks with a single hidden layer ([Qian and Sejnowski \(1988\)](#); [Bohr et al.; Rost and Sander \(1993\)](#)) and two such networks stacked at most ([Jones \(1999\)](#); [Dor and Zhou \(2007\)](#)). A new generation of deep learning started recently with [Zhou and Troyanskaya \(2014\)](#) building Generative Stochastic Network with two hidden layers and later works that already include five or more, with some even reaching more than 30 ([Fang et al. \(2017a,b\)](#)). These deeper models introduced new major improvements while being more flexible in merging information from local and more distant contexts. Earlier approaches typically used the n-grams or sliding window approach. CNNs, although with a similar principle, have a rather pyramidal structure, being able to increase the span of their action (see Figure 2.7). RNNs can capture even longer interactions and are deep in the sense of having the information at one timestep repeatedly re-processed in many later timesteps. Table 2.2 collects the best results achieved for Q8 in the last few years. All results are measured on the CB513 benchmark dataset first introduced by [Zhou and Troyanskaya \(2014\)](#). All state-of-the-art algorithms are based on deep learning networks, either in the form of CNNs, RNNs, or both combined.

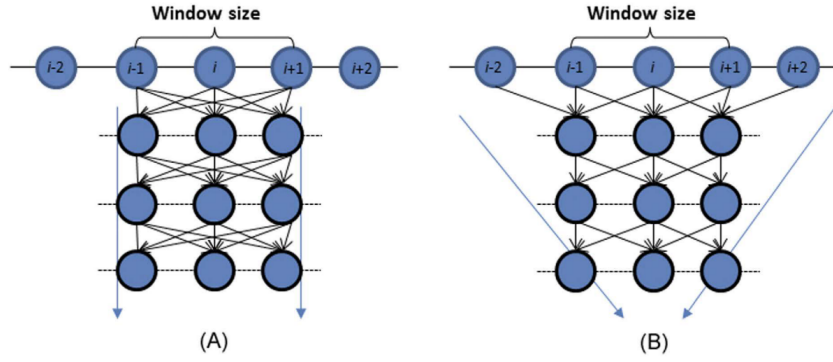


FIGURE 2.7: *Improvements of CNNs over fixed-window sliding*. While fixed-window MLPs are not as flexible when capturing information from different contexts (left), CNNs are able to merge local information at the lower layers with longer-range info at upper layers (Busia and Jaitly (2017)). Furthermore, increasing their depth expands the window size without adding much complexity to the model. Figure reproduced from Wang et al. (2016).

Names	Q8	Architecture	Date
Zhou and Troyanskaya (2014)	66.4%	CGSN	2014
Magnan and Baldi (2014)	66.5%	SSPro (BRNN)	2014
Sønderby and Winther (2014)	67.45%	LSTM	2014
Wang et al. (2016)	68.3%	DeepCNF	Jan 2016
Li and Yu (2016)	69.7%	DCRNN	Apr 2016
Lin et al. (2016)	68.4%	MUST-CNN	May 2016
Busia and Jaitly (2017)	71.4%	Deep3I+conditioning	Feb 2017
Hattori et al. (2017)	68.0%	DBLSTM	May 2017
Jurtz et al. (2017)	70.2%	LSTM+CNN	Aug 2017
Johansen et al. (2017)	70.9%	BGRU-CRF	Aug 2017
Fang et al. (2017a)	71.1%	DeepNRN+Deep3I	Nov 2017
Zhou et al. (2018)	70.3%	CNN+highway	Jan 2018
Fang et al. (2017b)	70.63%	MUFold-SS (Deep3I)	Feb 2018

TABLE 2.2: *State-of-the-art Q8 results on benchmark CB513*. All networks have some sort of deep learning architecture. Architectures in bold include CNNs. The two best Q8 results are marked in bold.

Chapter 3

Methods

Most of the computation work is performed on the *IRIDIS High-Performance Computing Facility*, with the help of associated support services at the university. They make use of NVIDIA® GeForce GTX 1080 Ti Graphical Processing Units (*GPUs*). The integration of GPUs has been possible thanks to the CUDA 9.0 toolkit¹.

3.1 Dataset

This project uses the database produced and made public by Zhou and Troyanskaya (2014)². This database has been taken as the flagship benchmark since its release, and its use allows fair comparisons with most state-of-the-art algorithms. It includes two sub-sets (training and test) of proteins that come from different sources, ensuring that the test set is composed of completely new samples. For this same purpose, they filtered the training set, stripping out every sequence that held 25% or more similarity with any protein from the test set. The training set was obtained from PISCES server (Wang and Dunbrack (2003))³ from a date before January 2014, which was in time culled from the Protein Data Bank (PDB) (Berman et al. (2003)). It has an original size of 6133 that gets reduced to 5534 after the filtering. The test set comes from the CB513 dataset (Cuff and Barton (1999)) and includes 514 sequences⁴.

Protein sequences can be up to 700 amino acids long (with an average of about 214) and have already been pre-processed by Zhou and Troyanskaya (2014), with one-hot encoded amino-acids along with the 21-long vector of *pssm* values as inputs, and their one-hot secondary structure Q8 classes as targets. The appearance frequencies of each class in both datasets are shown in Figure 3.1.

¹<https://developer.nvidia.com/cuda-toolkit>

²It can be accessed at <https://www.princeton.edu/~7Ejzthree/datasets/ICML2014/>

³http://dunbrack.fccc.edu/Guoli/PISCES_OptionPage.php

⁴Originally 513, but the last one was split in two since it was longer than the 700 amino-acids limit.

FREQUENCY DISTRIBUTION

Freq. Train (%)	Freq. Test (%)	Class	
34.535	30.85	H	(α -helix)
21.781	21.25	E	(β -strand)
19.185	21.14	L	(loop)
11.284	11.81	T	(β -turn)
8.258	9.81	S	(bend)
3.911	3.69	G	(3_{10} -helix)
1.029	1.39	B	(β -bridge)
0,018	0.03	I	(π -helix)

TABLE 3.1: Target frequencies on the CB6133 (left) and the CB513 (right). Table reproduced from [Hattori et al. \(2017\)](#).

A subset of 256 proteins was taken out of the training set and used for validation, leaving 5278 proteins for the training. This splitting is common in previous papers ([Zhou and Troyanskaya \(2014\)](#); [Sønderby and Winther \(2014\)](#); [Busia and Jaitly \(2017\)](#); [Jurtz et al. \(2017\)](#); [Hattori et al. \(2017\)](#)).

3.2 Network of study

The interpretability methods could be applied to any state-of-the-art network, as these would provide the most refined information about the secondary structure problem. However, in order to reach peak accuracies, these models are incredibly huge and not handy to work on, especially when it comes to computational time. For this reason, a simpler network is produced and employed for this analysis, with the hope that it will not lose generality over more complex networks.

The network that is used in this study has been built and trained using the open-source code developed by [Jurtz et al. \(2017\)](#)⁵ on the *Lasagne* framework ([Dieleman et al. \(2015\)](#)). While most training configurations are preserved (cross-entropy with L2 regularisation as the error function, batch normalisation, uniform glorot initialisation, mini-batches of size 64, RMSprop rule updates, gradient clipping), the network architecture itself has been completely rebuilt for this project. The weights for the final model are the ones from the epoch that has the best performance on the validation set.

The network is composed of three successive convolutional networks and a dense layer on top. Each of the convolutional layers contains three sets of filters of size 3, 5 and 7, respectively, with 16 filters per size. There are skip connections that by-pass every convolutional network in the same fashion as *ResNet* ([He et al. \(2015\)](#)), so the dense layer gets the concatenation of the raw input along with the outputs from the first, second and third layer altogether. The dense layer has 200 neurons and is connected to a *soft-max* layer that outputs the secondary structure prediction. The convolution operation is carried out with padding at each end of the sequence to preserve the length

⁵ Accessible at <https://github.com/vanessajurtz/lasagne4bio>.

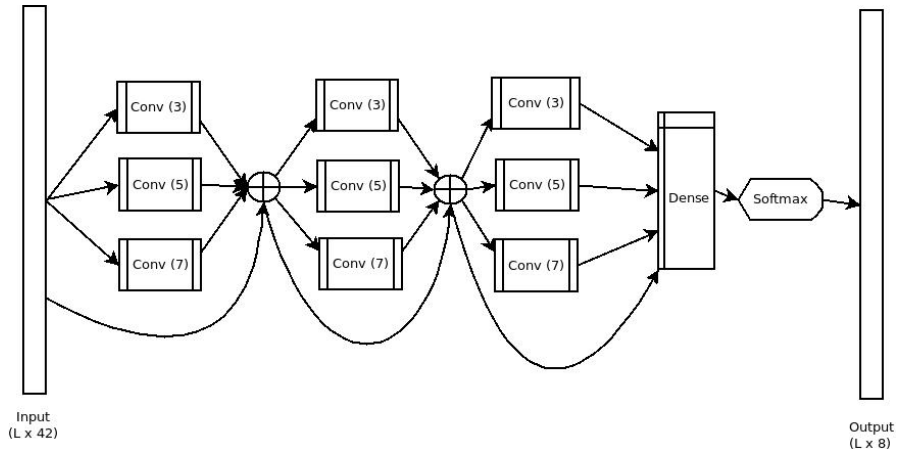


FIGURE 3.1: *Schema of network architecture.* There are three convolutional layers with filters of size 3, 5 and 7, followed by a dense layer and the softmax. Skip-connections bring together the output from all previous layers to each new layer.

of the sequences throughout the convolutional layers and produce in the final step one label per position. A sketch of the network can be seen in Figure 3.1.

The total window size for this network is 19, meaning that for making a single secondary structure classification the network obtains information from 9 adjacent positions at each side. Although some authors claim that the network should capture long interactions between amino-acids (Li and Yu (2016); Lin et al. (2016); Hattori et al. (2017); Heffernan et al. (2017)), it has been proven that most relevant information comes from the local environment (Busia and Jaitly (2017)), so the limited window size should not impinge the model performance. This fact also supports the idea that the skip connections are beneficial since they avoid the most local information to be “washed out” in upper layers (Busia and Jaitly (2017)).

3.3 Feature visualization

This work only uses first-layer filters as feature visualisation method. These only give a minimal amount of information about the very first features created, with a hard interpretation due to the high depth of the network. In this case, we have filters with three different sizes to inspect: 3x42, 5x42 and 7x42. They can be visualized in a intuitive way in the form of *sequence logos*, which can be generated with the *Seq2Logo* tool (Thomsen and Nielsen (2012)). Other feature visualisation techniques remain for future work.

3.4 Saliency maps

Saliency maps have been calculated by the conventional technique of computing the gradient of the output with respect to the inputs and multiplying it by the value of the input itself ([Shrikumar et al. \(2016\)](#)). A significant difference between this work and most previous papers that make use of saliency maps is that they perform many-to-one classification (one output class per sequence/image) and here the classification task is many-to-many (each position of the sequence is assigned a class), producing many saliency maps for a single sequence. More specifically, every single position produces a saliency map that contains the influence of the 42-size input (21 amino-acids plus 21 *pssm* scores) onto the 8-size soft-max output. This information covers the 19 positions surrounding the one being predicted, ending up with a saliency map with total dimension 8x42x19. They are computed using the Theano framework ([The Theano Development Team et al. \(2016\)](#)) since it allows automatic differentiation of symbolical expressions and the use of GPUs.

3.4.1 Extracting information from saliency maps

The presence of overlapping saliency maps allows for different ways of aggregating them to extract meaningful information. In order to obtain information for a specific sequence, the overlapping saliency maps of such sequence could just be added up, resulting in a single, long *sequence-specific* saliency map of size 8x42x l .

By changing the focus to general information of the network behaviour, the sheer addition of all saliency maps would produce a single 8x42x19 map showing the average behaviour. From this map we could extract information about the general behaviour of a particular class (*class-specific* saliency map) or a certain amino-acid (*pssm-specific* saliency map). If a more fine-grained inspection is desired, clustering techniques can be used, and every cluster creates their independent 8x42x19 representative map by addition of all their components.

3.5 Open-source

As it is the standard practice in both the bioinformatics and machine learning research communities, all the code from this project has been released as open-source on the web platform GitHub and can be accessed through the URL <https://github.com/Juillermo/lasagne4bio>, with the hope that the tools developed here can be of use for future research.

Chapter 4

Results & Discussion

I have trained the network described in Section 3.2 for 400 epochs with the same parameters as the ones used by [Jurtz et al. \(2017\)](#); i.e., gradient clipping at 20, regularisation term $\lambda = 10^{-4}$, learning rate varying from $\mu = 0.025$ down to 10^{-4} throughout the epochs. The resulting network reaches an accuracy of 67.74% on the test set, which is not far from the 71% of the state-of-the-art (see Table 2.2). I believe that the techniques of analysis here presented and the conclusions withdrawn from them can be transferred to current state-of-the-art methods without losing validity.

4.1 Outlier analysis

In order to analyse the performance space a bit better, the average accuracy per sequence has been calculated, and it has been plotted with respect to their sequence length in Figure 4.1. The distribution exhibits the typical funnel shape that one could expect from processes with random variables, forming groups of different sizes: the bigger the groups, the smaller the variance. The funnel ceases to shrink at about 400 length, so it would be particularly attractive to understand why the network is classifying worse (60% and below) some of the sequences above that length.

If we observe the colour scheme in the figure, we can see that sequences rich in α -helix are generally better predicted than β -sheets and coils. An explanation could be that while α -helix sizes are up to five positions away, which is inside the window size, β -sheets interact with amino-acids further away in the sequence, which is not possible to be captured with the window of the network, of lateral size of nine. This is in line with previous literature ([Rost \(2001\)](#)).

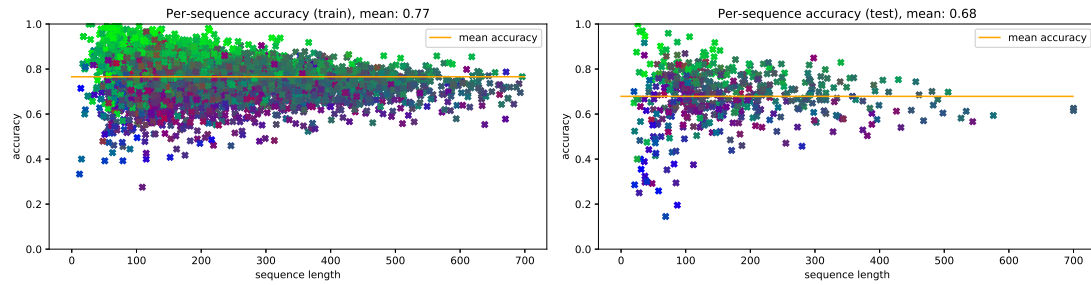


FIGURE 4.1: *The mean accuracy per sequence by sequence length.* The 5504 sequences of the training set are shown on the left and the 514 of the test set on the right. Each point represents a single protein, and its colour corresponds to the amount of β -sheets (red), α -helices (green), and coils (blue) it has. A purple point, for instance, would predominantly have β -sheets and coils.

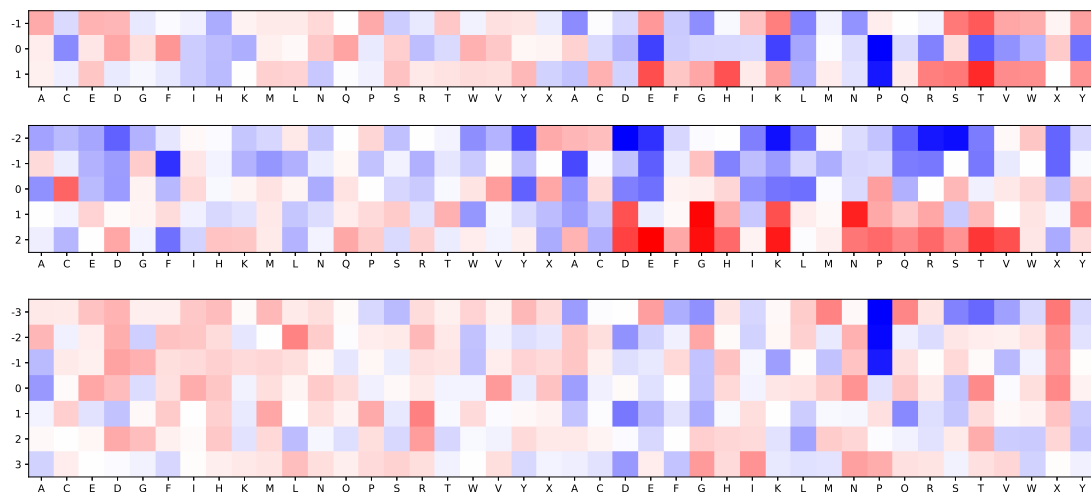


FIGURE 4.2: *Three sample first-layer filters, each of a different size.* The y axis shows is the window of the filter and the x axis the depth of the input, with the 21 first positions on the left corresponding to the one-hot encoding amino-acids and the right 21 positions to the *pssm scores*. Positive values are in red and negative values in blue.

4.2 Feature visualization: first-layer filters

Some first-layer filters are shown in Figure 4.2. The first thing to notice is that for the upper two filters the side corresponding to $pssm$ contains stronger values, so filters seem to be focusing more on them. Although this asymmetry is not present in all filters, it seems to be prevalent in most of them. The middle filter (size five) has the features of an edge detector for specific $pssm$ values: these need to be at the right side and not at the left side for the filter to give a higher output. The bottom filter (size seven) heavily penalises P values on the left. All the filters from the first layer can be seen in Appendix A. Two filters in *Seq2Logo* form can be seen in Figure 2.5.

4.3 Saliency maps on inputs

Before going through the analysis, it is worth recalling that the saliency map outputs have dimensions $8 \times 42 \times 19$ for each position at each sequence, corresponding to the eight classes (outputs), the 42 inputs and the total window size of 19 (as explained in Section 3.4).

4.3.1 Analysis of amino-acids and *pssm*

When looking at standard secondary-structure prediction algorithm, there is one point that may raise some suspicion: the inclusion of half of the inputs as one-hot encoded (amino-acids) and the other half as dense vectors (*pssm*). One could think that this discrepancy may strongly favour the information coming from the dense part since the weights associated to it will learn much faster in a typical gradient descent learning schema.

Saliency maps can be used to prove whether this hypothesis is right by inspecting which of the input groups is being most decisive in the classification process. For doing so, each saliency map is divided into two groups of $8 \times 21 \times 19$, one corresponding to the values for one-hot amino-acids and the other for the *pssm* inputs, and all the values inside each group are added up in absolute value to a single **saliency score**. Thus, each position of each sequence will have two scores, one for the amino-acids and one for the *pssm*, and its comparison will tell us to which extent each part of the inputs were relevant for making a classification.

Only a single case out of the close to 1.3 million positions showed a higher one-hot than *pssm* score and the difference only accounted for 1% of their value. The rest of the scores were in favour of the *pssm* saliency, with the distribution shown in Figure 4.3. From the figure, we can know that almost the totality of the *pssm* scores were at least four times bigger than the one-hot ones, and therefore we can solidly confirm that the influence of the one-hot data on the input is minor and its omission would not cause much loss in the performance of the network. To prove so, a second network has been trained with the same settings as the original one but only with *pssm* as input data. Its accuracy was 67.58%, 0.16% lower than the original system. The difference could be a result of statistical variance, so further runs would need to be carried out to obtain a statistically significant result. Because of these findings, the rest of the chapter will focus only on the effect of the *pssm* on classification.

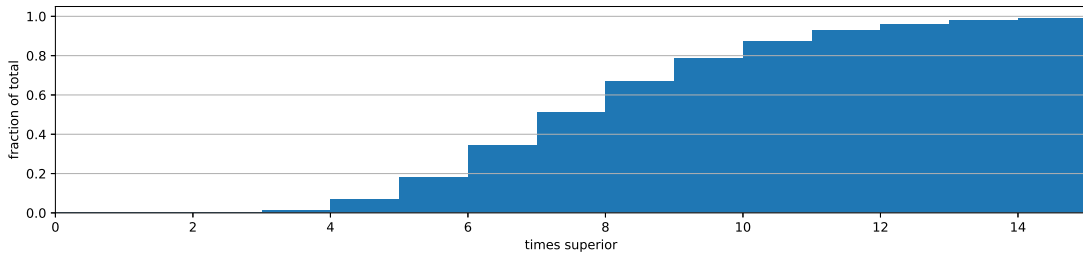


FIGURE 4.3: *Pssm saliency superiority*. This figure shows a cumulative histogram of the number of positions whose *pssm* saliency score was higher than the one-hot score. The *x* axis represent the superiority ratio, i.e. how many times bigger was the score.

4.3.2 Sequence-specific saliency maps

This section will present the sort of analysis that can be done for a specific sequence. It can be especially useful for analysing the sequences whose accuracy was remarkably lower (outliers). Each sequence has a number of saliency maps equal to its length, l , and they can either be inspected one by one or be overlapped through the sequence, obtaining a single 8x42xl **sequence map**.

Figure 4.4 shows consecutive saliency maps belonging to a single class. The patterns they present are generally preserved (note the differences in scales), just being shifted by one position on the window axis. It suggests that the algorithm is not differentiating that much between specific amino-acid positions, but instead looking for them to be in the vicinity. For this reason, we can consider that overlapping them in a single sequence map does preserve most of the information, as it is shown in Figure 4.5. This sort of map reveals which amino-acids of the vicinity are mostly responsible for a prediction in a particular position. For instance, the predictions of class *E* on the left side of the shown fragment have to do with the presence of amino-acids *A*, *V* and *L*, while the failure to predict class *H* on position 109 is likely related to the presence of amino-acid *D* at position 110. Note that these saliency values come from the *pssm* side, which explains why positions 105 and 106 have different values despite having the same amino-acid (*D*). It is especially important to take this into account since we have discussed before that one-hot amino-acid information is not as decisive for making the predictions.

Another issue worth noting is a non-realistic inconsistency among predictions: the algorithm assigns labels individually per-position and does not take into account the labels it is providing at the sides. It leads to situations such as having individual *G*s when these only come at least in groups of three. Different approaches in the state-of-the-art for dealing with this are adding a *struct2struct* machine on top of the predictions (Rost and Sander (1993); Fang et al. (2017b)), iterative processes that learn from previous step's prediction (Heffernan et al. (2017)), or probabilistic methods that convey information about adjacent positions, like *Conditional random fields* Wang et al. (2016) or *next-step conditioning* Busia and Jaitly (2017).

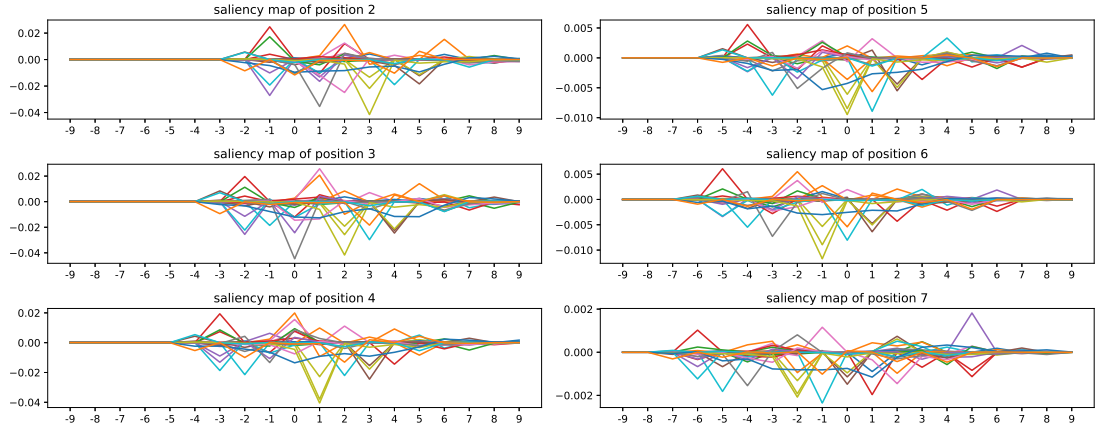


FIGURE 4.4: *Saliency maps for consecutive positions in a sequence*. In every sub-figure there are 42 lines of the 42 inputs, corresponding to their saliency values for class H .

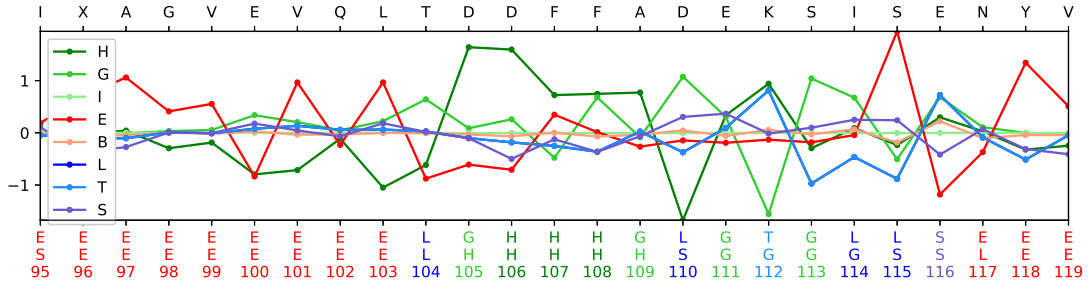


FIGURE 4.5: *Fragment of a sequence map aggregated by the input*. Each line corresponds to the aggregated saliency values of one of the eight output classes. The upper x axis displays the amino-acids in the sequence. The lower x axis contains three sets of labels in this order: the predictions, the true values, and the positions in the sequence. The code of colours of the labels is the same as the lines and is set according to the class of the predictions.

For a more in-depth look into the whole *pssm* spectrum, we would need to narrow down the scope to a single class, as it is done in Figure 4.6. This figure reveals that it is indeed common that the real amino-acid in the sequence is not among the most influential ones from the *pssm* for making the decision. Note that the *pssm* values of the amino-acids do not always need to have contributions of the same sign (such as *P* or *D* in the figure), revealing that the network is capturing something more than a pure presence: location and combinations of amino acids are also prominent.

4.3.3 Class-specific and pssm-specific saliency maps

Instead of looking at the saliency information along single sequences, aggregating the information from all the 1.3 million saliency maps could give us some broader information of what the network has learned. Again, the high dimensionality of the data to explore requires us to seek meaningful ways to aggregate and represent the data.

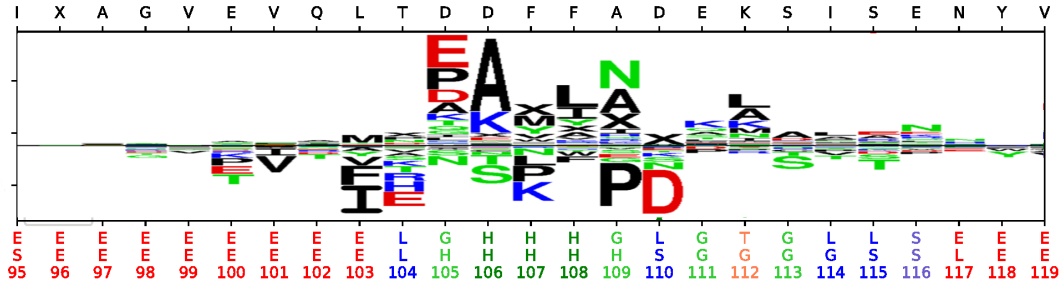


FIGURE 4.6: Fragment of sequence map for class *H* in sequence logo form. The saliency of the *pssm* values is shown here. The frame and labels of the figure is the same as in Figure 4.5. The image has been generated by *Seq2Logo* Thomsen and Nielsen (2012).

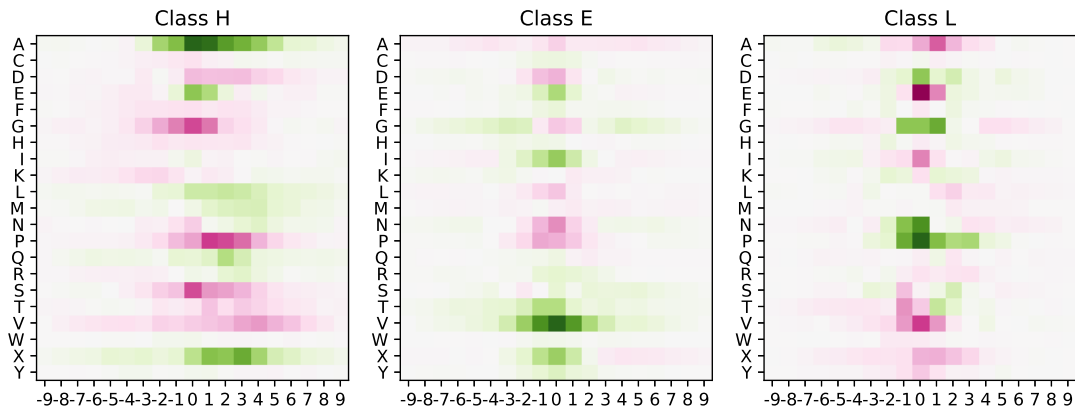


FIGURE 4.7: Per-class aggregated saliency maps of the main three classes along the window. Only the saliency values of *pssm* are shown here. Green means positive saliency values and purple means negative.

Sheer addition

A simple way to aggregate the saliency maps would be adding them up with element-wise addition, thus composing a single saliency map of size $8 \times 42 \times 19$. This mega-saliency map should convey rough information of the general features of the network.

To start with, Figure 4.7 shows the aggregated class-specific saliency maps for the three main classes and the 21 *pssm* values. There are a few details to notice here. First, higher saliency values concentrate around the centre of the window, meaning that most relevant information is located around five positions from the predicted one. However, class *H* shows a slight skewness towards the right; it focuses more on what further positions contain than what was before. Second, most *pssm* values preserve the same sign along the window of a class, although exceptions also occur. Third, as it could be expected, class *L* generally presents inverse patterns with respect to classes *H* and *E*. It makes sense since coils appear wherever there are no α -helices or β -strands, they are complementary. Lastly, each class has a “feature” *pssm* value that is their best indicator: *A* for class *H*; *V* for *E*; and *P* for *L*.

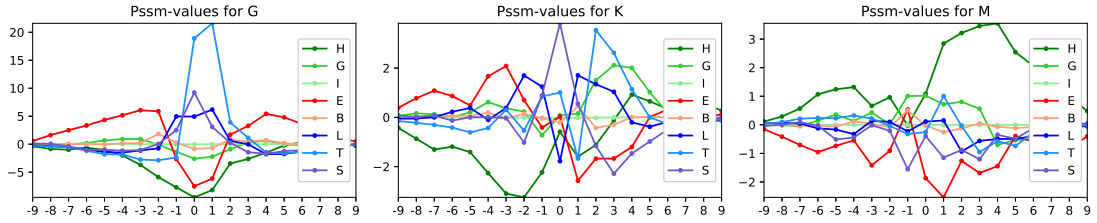


FIGURE 4.8: *Per-class aggregated saliency map of amino-acids G, K, and M, in this order. Y axis is in 1000s. Note the change in scale, particularly for the left-most plot (amino-acid G).*

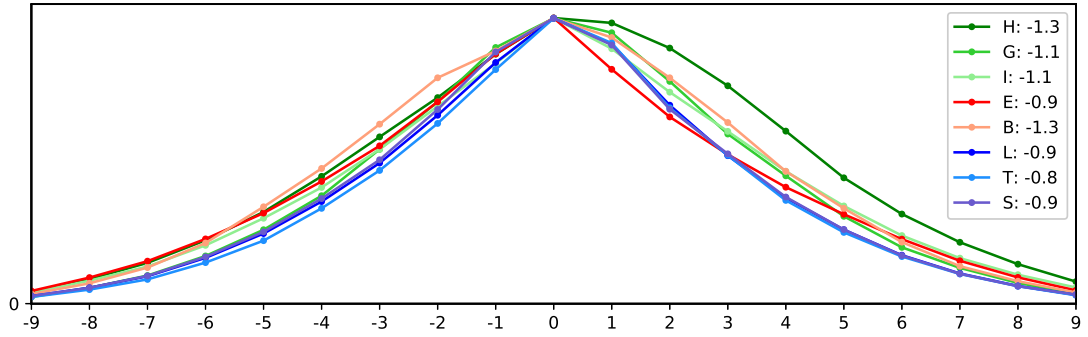


FIGURE 4.9: *Classes overall influence along the window size. All lines are normalized to have the same height, as the analysis focuses on the shapes rather than the values. Labels include a measurement of the kurtosis of the distributions.*

Figure 4.8 shows the same information but from a different perspective: as it is *pssm-specific*, it focuses on how a single *pssm*'s position affects the classification on the eight classes. These plots show important effects of the position, as all of them make significant shifts at the centre of the window. *Pssm* value *G* strongly favours coils around its position but foresees the presence of β -strands a few positions away in either side. *Pssm* value *K* has a more chaotic effect with high asymmetry: while favouring β -strands and hindering helices on the left, it switches this behaviour on the right and favours coils as well. *Pssm* value *M* is generally favouring α -helices, although 3_{10} -helices gain importance at the very centre. The skewness of α -helices to the right is quite evident here. Note the difference in scales, which indicates that *pssm*-values of *G* are in any case more influential than the other two.

Lastly, we can use the aggregated saliency maps to investigate the span of a class influence, i.e. how much of the further away positions the network uses to predict the class. For performing this analysis, the addition of the saliency maps must be done in absolute value and then aggregated by the *pssm* dimension. Figure 4.9 reveals the results for this operation. Helices and strands have higher side influence, as it could be expected. They all present a moderate level of asymmetry, with more variance happening on the right side, with α -helices (*H*) paying more attention to side positions and β -strands (*E*) focusing less on side positions.

4.4 Final discussion

The results shown here are a small sub-sample of the kind of information that can be obtained from saliency maps. An exhaustive catalogue including plots for all classes and $pssm$ values can be found in Appendix B.

The asymmetry in the saliency maps requires further discussion. It seems it is natural to have some degree of asymmetry since we only count with a sub-sample of data and there can be some statistical variation. However, the consistency in the skewness suggests that there is some stronger underlying reason for this. The ribosome creates amino-acids sequentially, and it could be argued that the free end is already dynamically folding into their secondary structure while the amino-acids are still being assembled at the other end. So in the case of the α -helix, the amino-acids coming after the one being inspected would determine more whether some folding is going to occur than the ones previously released. A bit more of time should be employed into determining whether this idea is consistent with what is known about protein formation.

The analysis performed on Section 4.3.3 can be subject to criticism for other reasons. It mostly shows the influences of single amino-acids and their positions on specific classes. One could imagine a simple statistical linear model that looks at the frequencies in the training set that specific amino-acids are at certain positions with respect to specific classes and maybe we would get similar results. It is clear that CNNs are doing more than that, as their improved performance can prove. A direct comparison between both algorithms would shed more light on what the CNN is learning out of statistics from single amino-acids. Another way of doing so is not just focusing on the influence of single amino-acids but combinations of them. Since inspecting all the combinations of amino-acids and positions would be endless, other smarter approaches would need to be taken for doing so. One of them could be applying clustering on the saliency maps, with the hope that there are few strong modes (e.g. class H being activated mostly when four specific combinations happen). Another approach could be implementing the feature visualisation technique of activation maximisation, as explained in Section 2.2.1.

The theoretical discussion of saliency maps in Section 3.4 introduced the state-of-the-art techniques for building them. This work has applied the gradient * input approach, as it leverages simplicity and effectiveness. Although more recent techniques for calculating saliency maps proved to have better results, the whole framework for aggregating and evaluating them still holds and is independent of how the saliency maps were calculated.

The choice of protein secondary structure prediction is rooted in that it is a well-known problem. There has been some discussion on whether it is the best middle-step for reaching 3D structures, based on the fact that classification of secondary structure in these eight types has some degree of arbitrariness. The main alternative is predicting the angles of the backbone between every two amino-acids, transforming the problem

from classification to regression. While translating the techniques developed here to this new problem is not straightforward, significant parts of it —as the ideas for aggregating saliency maps— can be recycled and adapted to the new context.

Chapter 5

Conclusions

The field of biomedical research requires more than high accuracy; the ability to interpret models is also a valuable asset. Deep learning has increased the first point but fails at the second. Luckily, some interpretability techniques are being developed in the context of image processing and can be applied to other fields. This work has implemented for the first time saliency maps in a structure-to-structure sequential problem, namely, the protein secondary structure prediction problem. While saliency maps in problems with a single output per sequence are simple to interpret, structure-to-structure problems have more dimensions, so further methods for aggregating and inspecting them are also necessary. The aggregating methods shown here focus on sequences, inputs or outputs, uncovering different relations in the data. This type of analysis can be readily understood by experts in the field and provide them with valuable new information.

Preliminary inspection of the saliency map has reassured the superiority of *pssm* scores as inputs, later confirmed by an empirical experiment. Other relevant facts include the skewness of α -helices, which are influenced more strongly by the amino-acids coming afterwards. This asymmetry is also present in other classes and it varies depending on the *pssm* we look at. From a class-level perspective, α -helices have higher tendency to look at distant amino-acids (inside the limited window of 19); β -strands have more consideration for further positions as compared to other classes, but they still mainly focus on the close vicinity, so longer interactions does not seem to be captured by the network.

Still, further exploration techniques should be investigated. Other methods of aggregation can be explored since the ones here exposed only show features on a very general level. Clustering of the saliency maps would cover this aspect by including various facets of the features, and all techniques developed here can be applied independently to each of them and thus capture multi-modality. Feature visualisation techniques can also provide with extra valuable information, and their implementation should also be studied.

Finally, other kinds of problems can also be explored, such as backbone angle prediction, where the goal shifts from classification to regression.

Appendix A

First-layer filters

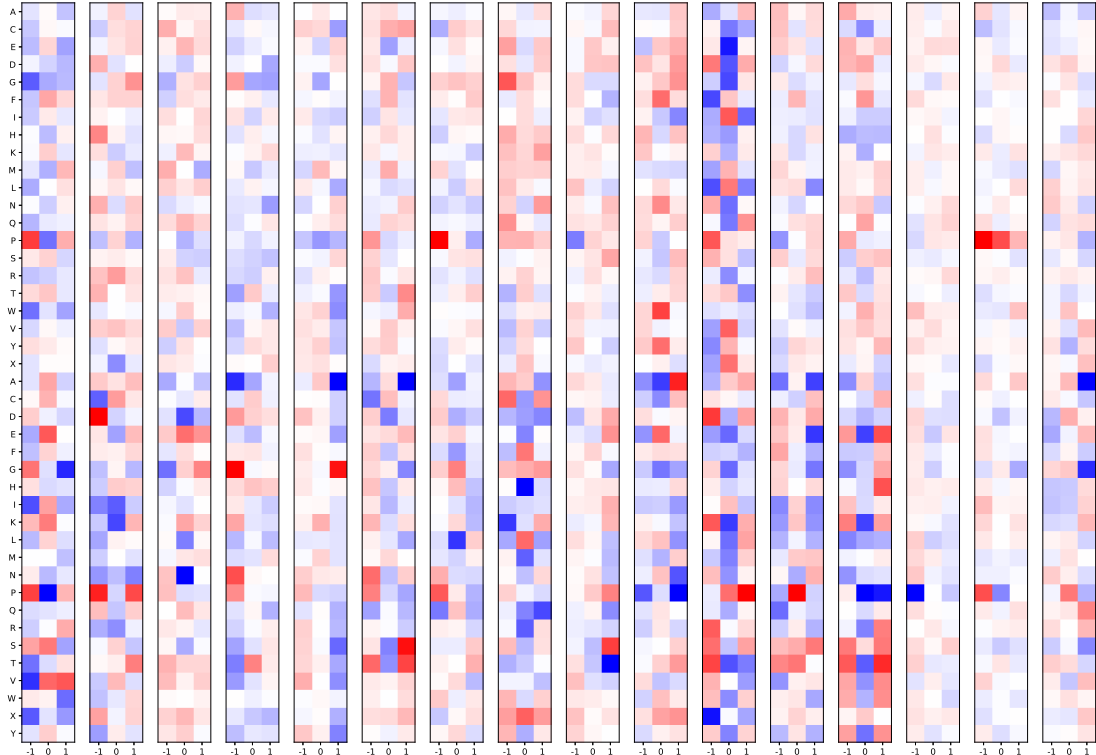


FIGURE A.1: *Filters of the first layer with size three.* The y axis is the depth of the network, with the upper 21 rows corresponding to the one-hot encoded amino-acids and the bottom 21 rows to the *pssm* values. x axis is the window size (width). Red values are positive and blue values are negative.

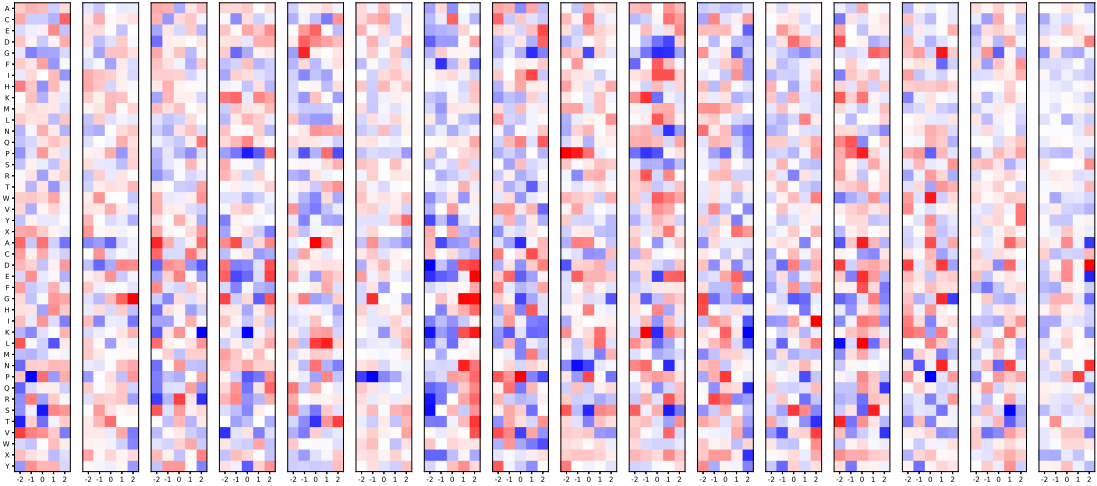


FIGURE A.2: *Filters of the first layer with size five.* The y axis is the depth of the network, with the upper 21 rows corresponding to the one-hot encoded amino-acids and the bottom 21 rows to the *pssm* values. x axis is the window size (width). Red values are positive and blue values are negative.

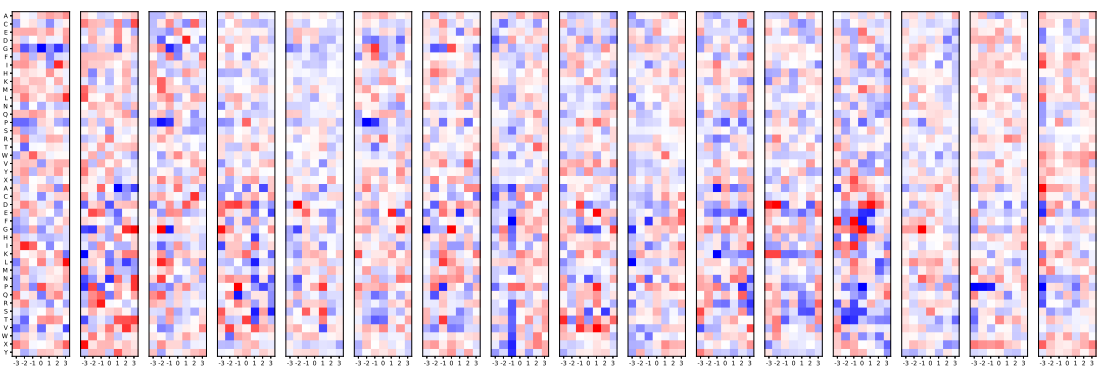


FIGURE A.3: *Filters of the first layer with size seven.* The y axis is the depth of the network, with the upper 21 rows corresponding to the one-hot encoded amino-acids and the bottom 21 rows to the *pssm* values. x axis is the window size (width). Red values are positive and blue values are negative.

Appendix B

Saliency map aggregations

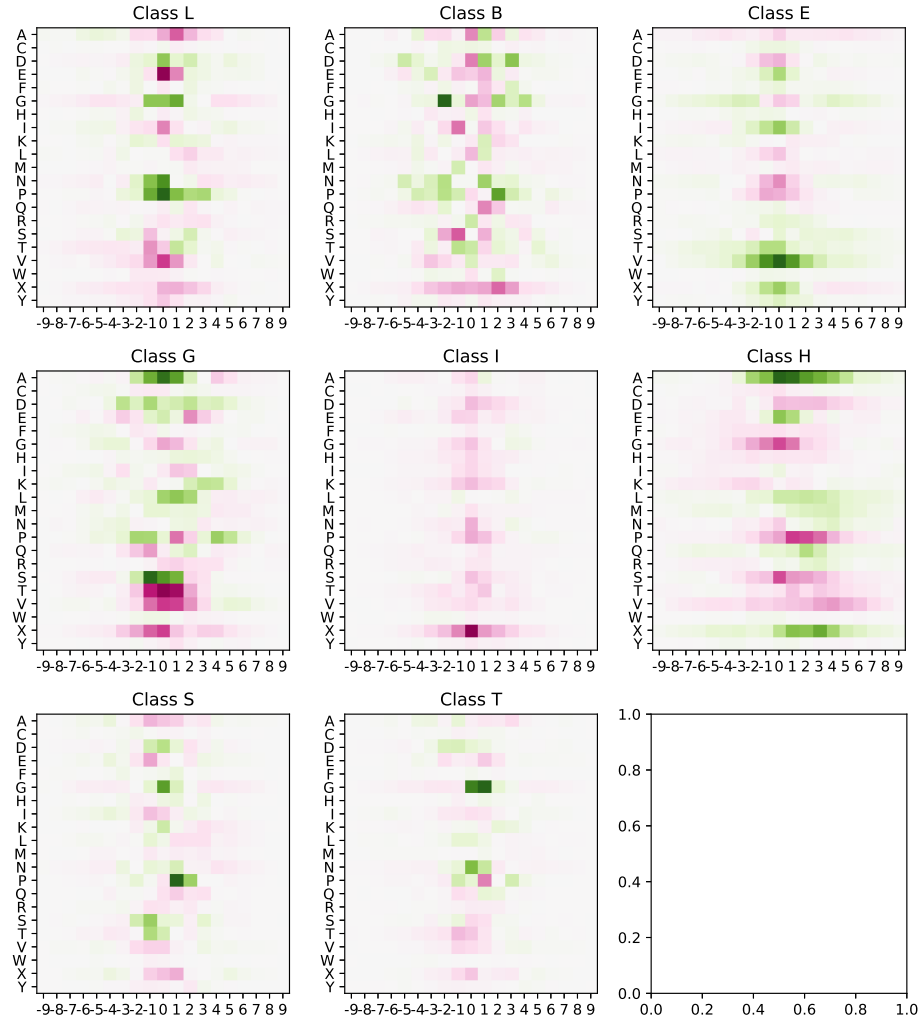


FIGURE B.1: *Per-class aggregated saliency maps along the window of all classes, as discussed in Section 4.3.3.* Only the saliency values of *pssm* are shown here. Green means positive saliency values and purple means negative.

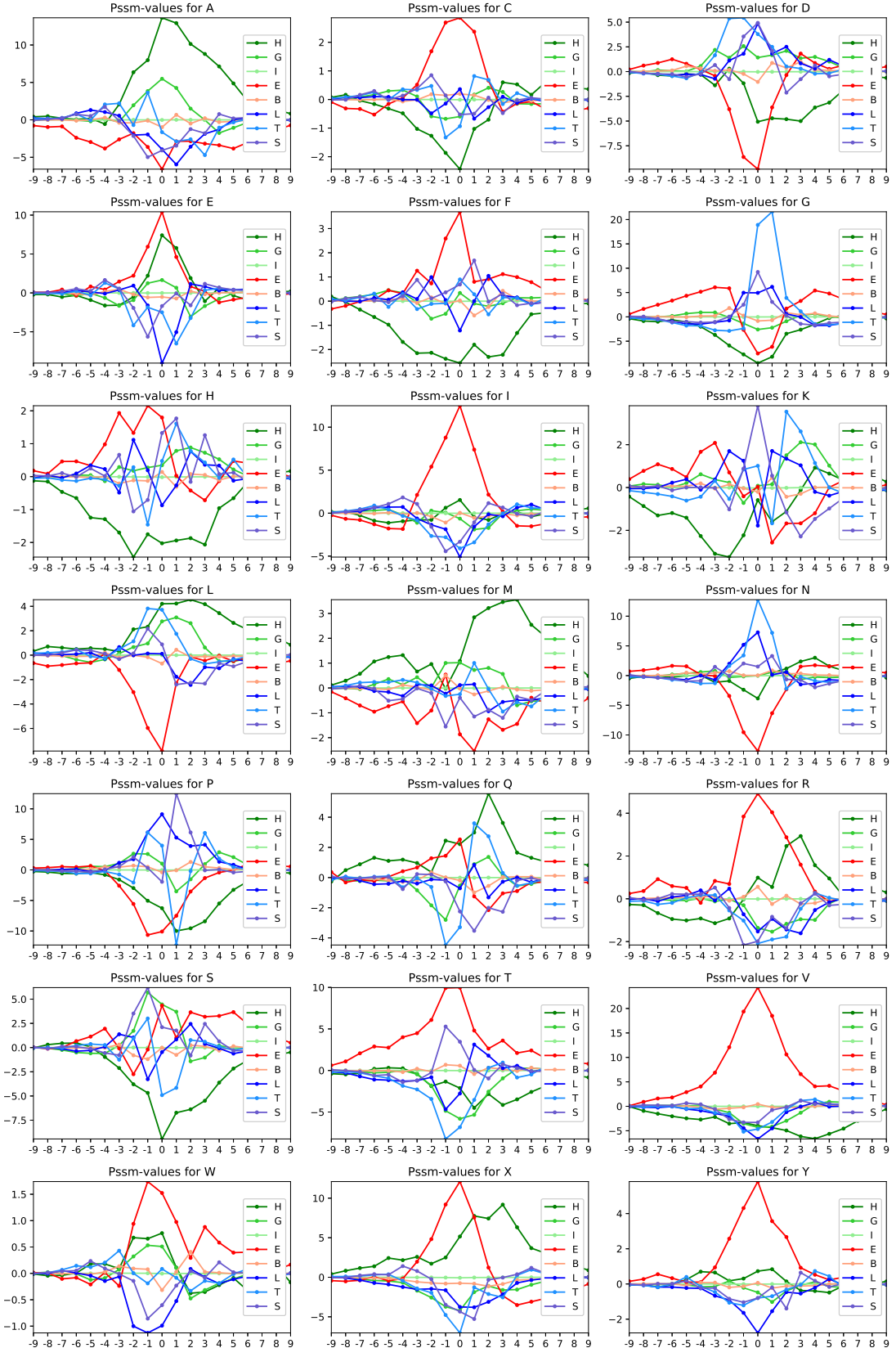


FIGURE B.2: *Per-class aggregated saliency map of all 21 amino-acids.* Y axis is in 1000s. Note the changes in scale.

Appendix C

Project planning

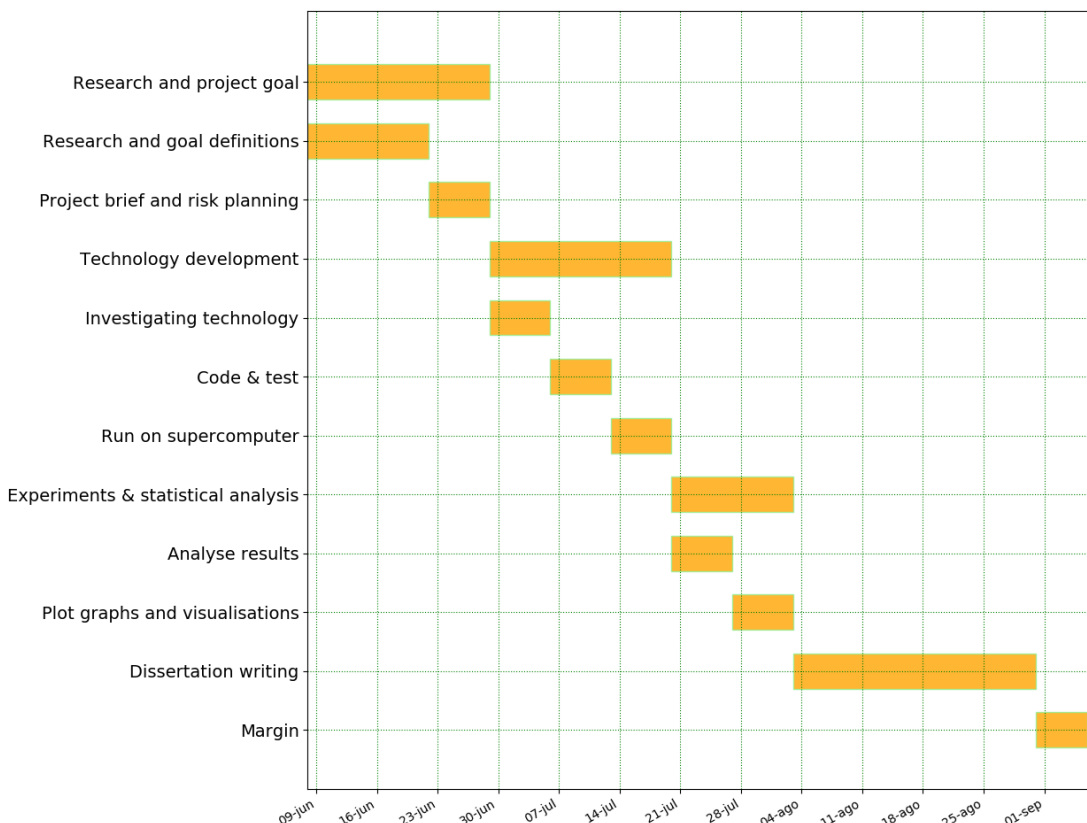


FIGURE C.1: *Gantt chart of the project planning*. Although the time was divided into four distinct phases (*Research*, *Technology development*, *Experiments*, and *Dissertation writing*), there has been some overlapping between them.

Bibliography

Babak Alipanahi, Andrew Delong, Matthew T. Weirauch, and Brendan J. Frey. Predicting the sequence specificities of DNA- and RNA-binding proteins by deep learning. *Nature Biotechnology*, 33(8):831–838, 2015. ISSN 15461696.

Stephen F. Altschul, Thomas L. Madden, Alejandro A. Schäffer, Jinghui Zhang, Zheng Zhang, Webb Miller, and David J. Lipman. Gapped BLAST and PSI-BLAST: A new generation of protein database search programs, 1997. ISSN 03051048.

Sebastian Bach, Alexander Binder, Grégoire Montavon, Frederick Klauschen, Klaus Robert Müller, and Wojciech Samek. On pixel-wise explanations for non-linear classifier decisions by layer-wise relevance propagation. *PLoS ONE*, 2015. ISSN 19326203.

Andrew R. Barron. Universal approximation bounds for superpositions of a sigmoidal function. *IEEE Transactions on Information Theory*, 1993. ISSN 00189448.

Helen Berman, Kim Henrick, and Haruki Nakamura. Announcing the worldwide Protein Data Bank, 2003. ISSN 10728368.

Henrik Bohr, Jakob Bohr, Sren Brunak, Rodney M.J. Cotterill, Benny Lautrup, Leif Nørskov, Ole H. Olsen, and Steffen B. Petersen. **Protein secondary structure and homology by neural networks the -helices in rhodopsin.** *FEBS Letters*, 241(1-2):223–228.

Akosua Busia and Navdeep Jaitly. Next-Step Conditioned Deep Convolutional Neural Networks Improve Protein Secondary Structure Prediction. *arXiv:1702.03865v1*, 2017.

Travers Ching, Daniel S. Himmelstein, Brett K. Beaulieu-Jones, Alexandr A. Kalinin, Brian T. Do, Gregory P. Way, Enrico Ferrero, Paul-Michael Agapow, Wei Xie, Gail L. Rosen, Benjamin J. Lengerich, Johnny Israeli, Jack Lanchantin, Stephen Woloszynek, Anne E. Carpenter, Avanti Shrikumar, Jinbo Xu, Evan M. Cofer, David J. Harris, Dave DeCaprio, Yanjun Qi, Anshul Kundaje, Yifan Peng, Laura K. Wiley, Marwin H. S. Segler, Anthony Gitter, and Casey S. Greene. *Opportunities And Obstacles For Deep Learning In Biology And Medicine*. 2017. ISBN 0000000305396.

- Kyunghyun Cho, Bart van Merriënboer, Caglar Gulcehre, Dzmitry Bahdanau, Fethi Bougares, Holger Schwenk, and Yoshua Bengio. [Learning Phrase Representations using RNN Encoder-Decoder for Statistical Machine Translation](#). jun 2014.
- Peter Y. Chou and Gerald D. Fasman. Prediction of Protein Conformation. *Biochemistry*, 1974. ISSN 15204995.
- J a Cuff and G J Barton. Evaluation and improvement of multiple sequence methods for protein secondary structure prediction. *Proteins*, 1999. ISSN 0887-3585.
- George Cybenko. Approximations by superpositions of sigmoidal functions. *Approximation Theory and its Applications*, 1989. ISSN 10009221.
- Sander Dieleman, Jan Schlüter, Colin Raffel, Eben Olson, Søren Kaae Sønderby, Daniel Nouri, Daniel Maturana, Martin Thoma, Eric Battenberg, Jack Kelly, Jeffrey De Fauw, Michael Heilman, Diogo149, Brian McFee, Hendrik Weideman, Takacsg84, Peterderivaz, Jon, Instagibbs, Dr Kashif Rasul, CongLiu, Britefury, and Jonas Degrave. Lasagne: First release., 2015.
- Ken A. Dill and Justin L. MacCallum. The protein-folding problem, 50 years on, 2012. ISSN 10959203.
- Ofer Dor and Yaoqi Zhou. Achieving 80% ten-fold cross-validated accuracy for secondary structure prediction by large-scale training. *Proteins: Structure, Function and Genetics*, 2007. ISSN 08873585.
- Vincent Dumoulin and Francesco Visin. [A guide to convolution arithmetic for deep learning](#). mar 2016.
- Dumitru Erhan, Yoshua Bengio, Aaron Courville, and Pascal Vincent. Visualizing higher-layer features of a deep network. *Bernoulli*, 2009.
- C. Fang, Y. Shang, and D. Xu. A new deep neighbor residual network for protein secondary structure prediction. In *2017 IEEE 29th International Conference on Tools with Artificial Intelligence (ICTAI)*, pages 66–71, Nov 2017a.
- Chao Fang, Yi Shang, and Dong Xu. [MUFold-SS: Protein Secondary Structure Prediction Using Deep Inception-Inside-Inception Networks](#). sep 2017b.
- Jean-Luc Fauchère, Marvin Charton, Lemont B Kier, Arie Verloop, and Vladimir Pliska. Amino acid side chain parameters for correlation studies in biology and pharmacology. *International Journal of Peptide and Protein Research*, 1988. ISSN 0367-8377.
- Alex Finnegan and Jun S. Song. Maximum entropy methods for extracting the learned features of deep neural networks. *PLoS Computational Biology*, 2017. ISSN 15537358.
- Alejandro Fontal. *Neural Networks for Subcellular Localization Prediction*. PhD thesis, Wageningen University & Research, 2017.

- Ian Goodfellow, Yoshua Bengio, and Aaron Courville. *Deep Learning*. MIT Press, 2016. <http://www.deeplearningbook.org>.
- Jiuxiang Gu, Zhenhua Wang, Jason Kuen, Liyang Ma, Amir Shahroudy, Bing Shuai, Ting Liu, Xingxing Wang, Li Wang, Gang Wang, Jianfei Cai, and Tsuhan Chen. Recent Advances in Convolutional Neural Networks. *Arxiv*, 2017. ISSN 16641078.
- Leandro Takeshi Hattori, Cesar Manuel Vargas Benitez, and Heitor Silverio Lopes. **A deep bidirectional long short-term memory approach applied to the protein secondary structure prediction problem**. In *2017 IEEE Latin American Conference on Computational Intelligence (LA-CCI)*, pages 1–6, 2017. ISBN 978-1-5386-3734-0.
- Kaiming He, Xiangyu Zhang, Shaoqing Ren, and Jian Sun. ResNet. *arXiv preprint arXiv:1512.03385v1*, 2015. ISSN 1664-1078.
- Rhys Heffernan, Yuedong Yang, Kuldip Paliwal, and Yaoqi Zhou. Capturing non-local interactions by long short-term memory bidirectional recurrent neural networks for improving prediction of protein secondary structure, backbone angles, contact numbers and solvent accessibility. *Bioinformatics*, 33(18):2842–2849, 2017. ISSN 14602059.
- Gao Huang, Zhuang Liu, Laurens Van Der Maaten, and Kilian Q. Weinberger. Densely connected convolutional networks. In *Proceedings - 30th IEEE Conference on Computer Vision and Pattern Recognition, CVPR 2017*, 2017. ISBN 9781538604571.
- Alexander Rosenberg Johansen, Casper Kaae Sønderby, Søren Kaae Sønderby, and Ole Winther. Deep Recurrent Conditional Random Field Network for Protein Secondary Prediction. In *Proceedings of the 8th ACM International Conference on Bioinformatics, Computational Biology, and Health Informatics - ACM-BCB '17*, 2017. ISBN 9781450347228.
- D. T. Jones. Protein secondary structure prediction based on position-specific scoring matrices. *J. Mol. Biol.*, 1999. ISSN 0022-2836.
- William Jones, Kaur Alasoo, Dmytro Fishman, and Leopold Parts. **Computational biology: deep learning**. *Emerging Topics in Life Sciences*, 1(3):257–274, 2017. ISSN 2397-8554.
- Vanessa Isabell Jurtz, Alexander Rosenberg Johansen, Morten Nielsen, Jose Juan Almagro Armenteros, Henrik Nielsen, Casper Kaae Sønderby, Ole Winther, and Søren Kaae Sønderby. An introduction to deep learning on biological sequence data: Examples and solutions. *Bioinformatics*, 33(22):3685–3690, 2017. ISSN 14602059.
- Wolfgang Kabsch and Christian Sander. Dictionary of protein secondary structure: Pattern recognition of hydrogenbonded and geometrical features. *Biopolymers*, 22(12):2577–2637, 1983. ISSN 10970282.

- David R. Kelley, Jasper Snoek, and John L. Rinn. Bassett: Learning the regulatory code of the accessible genome with deep convolutional neural networks. *Genome Research*, 2016. ISSN 15495469.
- Alex Krizhevsky, Ilya Sutskever, and Geoffrey E Hinton. [Imagenet classification with deep convolutional neural networks](#). In F. Pereira, C. J. C. Burges, L. Bottou, and K. Q. Weinberger, editors, *Advances in Neural Information Processing Systems 25*, pages 1097–1105. Curran Associates, Inc., 2012.
- Jack Lanchantin, Ritambhara Singh, Beilun Wang, and Yanjun Qi. Deep Motif Dashboard: Visualizing and Understanding Genomic Sequences Using Deep Neural Networks. 2016. ISSN 23356936.
- Yann LeCun, Léon Bottou, Yoshua Bengio, and Patrick Haffner. Gradient-based learning applied to document recognition. *Proceedings of the IEEE*, 1998. ISSN 00189219.
- Honglak Lee, Roger Grosse, Rajesh Ranganath, and Andrew Y. Ng. Convolutional deep belief networks for scalable unsupervised learning of hierarchical representations. In *Proceedings of the 26th Annual International Conference on Machine Learning - ICML '09*, 2009. ISBN 9781605585161.
- Zhen Li and Yizhou Yu. Protein Secondary Structure Prediction Using Cascaded Convolutional and Recurrent Neural Networks. In *Proceedings of the Twenty-Fifth International Joint Conference on Artificial Intelligence*, 2016. ISBN 978-1-57735-770-4.
- Zeming Lin, Jack Lanchantin, and Yanjun Qi. [MUST-CNN: A Multilayer Shift-and-Stitch Deep Convolutional Architecture for Sequence-based Protein Structure Prediction](#). may 2016.
- Christophe N. Magnan and Pierre Baldi. SSpro/ACCpro 5: Almost perfect prediction of protein secondary structure and relative solvent accessibility using profiles, machine learning and structural similarity. *Bioinformatics*, 2014. ISSN 14602059.
- Mufti Mahmud, Mohammed Shamim Kaiser, Amir Hussain, and Stefano Vassanelli. Applications of Deep Learning and Reinforcement Learning to Biological Data, 2018. ISSN 21622388.
- Polina Mamoshina, Armando Vieira, Evgeny Putin, and Alex Zhavoronkov. Applications of Deep Learning in Biomedicine, 2016. ISSN 15438392.
- Gregoire Mesnil, Yann Dauphin, Kaisheng Yao, Yoshua Bengio, Li Deng, Dilek Hakkani-Tur, Xiaodong He, Larry Heck, Gokhan Tur, Dong Yu, and Geoffrey Zweig. Using Recurrent Neural Networks for Slot Filling in Spoken Language Understanding. *IEEE/ACM Transactions on Audio, Speech, and Language Processing*, 2015. ISSN 2329-9290.

Seonwoo Min, Byunghan Lee, and Sungroh Yoon. Deep learning in bioinformatics, 2017. ISSN 14774054.

Grégoire Montavon, Sebastian Lapuschkin, Alexander Binder, Wojciech Samek, and Klaus Robert Müller. Explaining nonlinear classification decisions with deep Taylor decomposition. *Pattern Recognition*, 2017. ISSN 00313203.

Grégoire Montavon, Wojciech Samek, and Klaus Robert Müller. Methods for interpreting and understanding deep neural networks, 2018. ISSN 10512004.

Alexander Mordvintsev, Michael Tyka, and Christopher Olah. [Inceptionism: Going deeper into neural networks, google research blog](#), 2015.

Anh Nguyen, Jason Yosinski, and Jeff Clune. [Multifaceted Feature Visualization: Uncovering the Different Types of Features Learned By Each Neuron in Deep Neural Networks](#). feb 2016.

Chris Olah, Alexander Mordvintsev, and Ludwig Schubert. [Feature Visualization. Distill](#), 2017. ISSN 2476-0757.

L. Pauling, R. B. Corey, and H. R. Branson. The structure of proteins: Two hydrogen-bonded helical configurations of the polypeptide chain. *Proceedings of the National Academy of Sciences*, 1951. ISSN 0027-8424.

Ning Qian and Terrence J. Sejnowski. Predicting the secondary structure of globular proteins using neural network models. *Journal of Molecular Biology*, 1988. ISSN 00222836.

Daniel Quang and Xiaohui Xie. DanQ: A hybrid convolutional and recurrent deep neural network for quantifying the function of DNA sequences. *Nucleic Acids Research*, 2016. ISSN 13624962.

B Rost and C Sander. Improved prediction of protein secondary structure by use of sequence profiles and neural networks. *Proceedings of the National Academy of Sciences of the United States of America*, 1993. ISSN 0027-8424.

Burkhard Rost. Review: Protein secondary structure prediction continues to rise, 2001. ISSN 10478477.

Google Sergey Ioffe and Google Christian Szegedy. Batch Normalization. *Icml*, 2015. ISSN 10282092.

Avanti Shrikumar, Peyton Greenside, and Anshul Kundaje. [Learning Important Features Through Propagating Activation Differences](#). apr 2017.

Avanti Shrikumar, Peyton Greenside, Anna Shcherbina, and Anshul Kundaje. Not Just a Black Box: Learning Important Features Through Propagating Activation Differences. *arXiv:1605.01713 [cs]*, 2016. ISSN 1938-7228.

Karen Simonyan, Andrea Vedaldi, and Andrew Zisserman. Deep Inside Convolutional Networks: Visualising Image Classification Models and Saliency Maps. *arXiv.org*, 2014.

Søren Kaae Sønderby and Ole Winther. Protein Secondary Structure Prediction with Long Short Term Memory Networks. *arXiv:1412.7828*, 2014.

Matt Spencer, Jesse Eickholt, and Jianlin Cheng. A Deep Learning Network Approach to ab initio Protein Secondary Structure Prediction. *Ieee/Acm Transactions on Computational Biology and Bioinformatics*, 2015. ISSN 1545-5963.

Jost Tobias Springenberg, Alexey Dosovitskiy, Thomas Brox, and Martin Riedmiller. **Striving for Simplicity: The All Convolutional Net**. dec 2014.

Nitish Srivastava, Geoffrey Hinton, Alex Krizhevsky, Ilya Sutskever, and Ruslan Salakhutdinov. Dropout: A Simple Way to Prevent Neural Networks from Overfitting. *Journal of Machine Learning Research*, 2014. ISSN 15337928.

Mukund Sundararajan, Ankur Taly, and Qiqi Yan. Axiomatic Attribution for Deep Networks. 2017. ISSN 1938-7228.

Christian Szegedy, Sergey Ioffe, Vincent Vanhoucke, and Alex Alemi. Inception-v4, Inception-ResNet and the Impact of Residual Connections on Learning. 2016. ISSN 01678655.

The Theano Development Team, Rami Al-Rfou, Guillaume Alain, Amjad Almahairi, Christof Angermueller, Dzmitry Bahdanau, Nicolas Ballas, Frédéric Bastien, Justin Bayer, Anatoly Belikov, Alexander Belopolsky, Yoshua Bengio, Arnaud Bergeron, James Bergstra, Valentin Bisson, Josh Bleecher Snyder, Nicolas Bouchard, Nicolas Boulanger-Lewandowski, Xavier Bouthillier, Alexandre de Brébisson, Olivier Breuleux, Pierre-Luc Carrier, Kyunghyun Cho, Jan Chorowski, Paul Christiano, Tim Cooijmans, Marc-Alexandre Côté, Myriam Côté, Aaron Courville, Yann N. Dauphin, Olivier Delalleau, Julien Demouth, Guillaume Desjardins, Sander Dieleman, Laurent Dinh, Mélanie Ducoffe, Vincent Dumoulin, Samira Ebrahimi Kahou, Dumitru Erhan, Ziye Fan, Orhan Firat, Mathieu Germain, Xavier Glorot, Ian Goodfellow, Matt Graham, Caglar Gulcehre, Philippe Hamel, Iban Harlouchet, Jean-Philippe Heng, Balázs Hidasi, Sina Honari, Arjun Jain, Sébastien Jean, Kai Jia, Mikhail Korobov, Vivek Kulkarni, Alex Lamb, Pascal Lamblin, Eric Larsen, César Laurent, Sean Lee, Simon Lefrancois, Simon Lemieux, Nicholas Léonard, Zhouhan Lin, Jesse A. Livezey, Cory Lorenz, Jeremiah Lowin, Qianli Ma, Pierre-Antoine Manzagol, Olivier Mastropietro, Robert T. McGibbon, Roland Memisevic, Bart van Merriënboer, Vincent Michalski, Mehdi Mirza, Alberto Orlandi, Christopher Pal, Razvan Pascanu, Mohammad Pezeshki, Colin Raffel, Daniel Renshaw, Matthew Rocklin, Adriana Romero, Markus Roth, Peter Sadowski, John Salvatier, François Savard, Jan Schlüter, John Schulman, Gabriel Schwartz, Iulian Vlad Serban, Dmitriy Serdyuk, Samira Shabanian, Étienne

- Simon, Sigurd Spieckermann, S. Ramana Subramanyam, Jakub Sygnowski, Jérémie Tanguay, Gijs van Tulder, Joseph Turian, Sebastian Urban, Pascal Vincent, Francesco Visin, Harm de Vries, David Warde-Farley, Dustin J. Webb, Matthew Willson, Kelvin Xu, Lijun Xue, Li Yao, Saizheng Zhang, and Ying Zhang. [Theano: A Python framework for fast computation of mathematical expressions](#). *arXiv e-prints*, may 2016.
- Martin Christen Frolund Thomsen and Morten Nielsen. Seq2Logo: A method for construction and visualization of amino acid binding motifs and sequence profiles including sequence weighting, pseudo counts and two-sided representation of amino acid enrichment and depletion. *Nucleic Acids Research*, 40(W1), 2012. ISSN 03051048.
- Ramzan Kh Umarov and Victor V. Solovyev. Recognition of prokaryotic and eukaryotic promoters using convolutional deep learning neural networks. *PLoS ONE*, 12(2), 2017. ISSN 19326203.
- Karel Veselý, Arnab Ghoshal, Lukáš Burget, and Daniel Povey. Sequence-discriminative training of deep neural networks. In *Proceedings of the Annual Conference of the International Speech Communication Association, INTERSPEECH*, 2013. ISBN 9781479927562.
- Guoli Wang and Roland L. Dunbrack. PISCES: A protein sequence culling server. *Bioinformatics*, 2003. ISSN 13674803.
- Sheng Wang, Jian Peng, Jianzhu Ma, and Jinbo Xu. Protein Secondary Structure Prediction Using Deep Convolutional Neural Fields. *Scientific Reports*, 6, 2016. ISSN 20452322.
- Yuedong Yang, Jianzhao Gao, Jihua Wang, Rhys Heffernan, Jack Hanson, Kuldip Palival, and Yaoqi Zhou. Sixty-five years of the long march in protein secondary structure prediction: The final stretch? *Briefings in Bioinformatics*, 2018. ISSN 14774054.
- Matthew D. Zeiler and Rob Fergus. Visualizing and understanding convolutional networks. In *Lecture Notes in Computer Science (including subseries Lecture Notes in Artificial Intelligence and Lecture Notes in Bioinformatics)*, 2014. ISBN 9783319105895.
- Xiang Zhang, Junbo Zhao, and Yann LeCun. [Character-level Convolutional Networks for Text Classification](#). sep 2015.
- Jian Zhou and Olga G. Troyanskaya. Deep Supervised and Convolutional Generative Stochastic Network for Protein Secondary Structure Prediction. 2014.
- Jian Zhou and Olga G. Troyanskaya. Predicting effects of noncoding variants with deep learning-based sequence model. *Nature Methods*, 12(10):931–934, 2015. ISSN 15487105.
- Jiyun Zhou, Hongpeng Wang, Zhishan Zhao, Ruifeng Xu, and Qin Lu. CNNH_PSS: Protein 8-class secondary structure prediction by convolutional neural network with highway. *BMC Bioinformatics*, 2018. ISSN 14712105.